LA-12651-T
Thesis

UC-413
Issued: November 1993

Elastic Scattering of Pions from Tritium and ^{3}He in the Backward Hemisphere in the Region of the $\Delta_{33}(1232)$ Resonance

Scott K. Matthews*

*Graduate Research Assistant at Los Alamos Group MP-10 and N-2. The George Washington University, Department of Physics, Washington, DC 20052.

Los Alamos
NATIONAL LABORATORY
Los Alamos, New Mexico 87545

ACKNOWLEDGMENTS

Many people have taken time and effort beyond what was required, to help me understand some physics, and maybe produce something worthwhile; I would like to thank them here.

First, my advisor, Dr. Bill Briscoe, and my unofficial advisors, Dr. Steve Greene and Dr. Ben Nefkens, who have all tried to help me develop my abilities as well as my goals.

The faculty at The George Washington University have been good friends to me over the years, interested in my life as well as my work. I especially thank Dr. Herman Hobbs and Dr. Francisco Prats for their friendship and advice, and Dr. Barry Berman, Dr. Kalvir Dhuga and Dr. Morton Taragin, for their efforts on the experiments and analysis.

At Los Alamos, I have been made welcome in two groups, MP-10 and N-2. I thank the managements of these groups for providing me with resources and experience, and their members for their advice and comradarie.

Over the years I have been supported by N-2 as a Graduate Research Associat ·, by The George Washington University as a Teaching Fellow, and by the National Science Foundation, through the research grant of Bill Briscoe and collaborators, as a Research Assistant. I gratefully acknowledge the commitment of all of these to education and research.

Contents

1 Physics **1**

1.1 Introduction 1
1.2 The A = 3 System 1
1.3 The Pion-Nucleon System 2
1.4 Charge Symmetry 4
1.5 Ratios 6
1.6 Elastic Scattering 11
1.6.1 Coulomb Scattering 11
1.6.2 Nuclear Scattering 12
1.6.3 Pion-Nucleus Scattering 12
1.6.4 A Simple Calculation 16
1.6.5 The Optical Model 23
1.7 Other Calculations 24
1.8 Summary 36

2 Experimental Equipment and Setup **38**

2.1 Introduction 38
2.2 LAMPF 38
2.3 EPICS 39
2.3.1 Channel and Spectrometer 39
2.3.2 Wire Chambers 42
2.3.3 Calculated Quantities 43
2.3.4 Muon Rejector 45
2.4 EURYDICE 50
2.4.1 Target Geometry and Ray Tracing 54
2.4.2 Backscatter 69
2.5 The Targets 73
2.6 The Target Changer 73
2.7 Safety Measures 74
2.8 Summary 74

3 Data Reduction **75**

3.1 General Analysis Features 75
3.1.1 Yields and Cross Sections 75

3.1.2 Ratios . . . 76
3.1.3 Normalizations . . . 77
3.2 Gas Factor . . . 79
3.2.1 Decay Correction . . . 82
3.3 Spectrometer Calibration . . . 82
3.4 Muon Rejector . . . 87
3.5 Data . . . 89
3.5.1 What Was Measured . . . 89
3.5.2 Quality of the Data . . . 90
3.5.3 Statistical Variations . . . 93
3.6 Methods of Data Reduction . . . 96
3.6.1 Scaling . . . 96
3.6.2 Straight-Line Backgrounds . . . 97
3.6.3 Deuterium ratios . . . 103
3.7 Cross Sections . . . 108
3.8 Systematic Errors . . . 110
3.9 Summary . . . 111

4 Results **112**
4.1 Ratios . . . 112
4.1.1 The Ratios ρ^+ and ρ^- . . . 113
4.1.2 The Ratios r_1 and r_2 . . . 119
4.1.3 The Superratio . . . 125
4.2 Cross Sections . . . 130

5 Summary and Conclusion **139**

List of Tables

2.1 Acceptance Corrections 68

3.1 Target Weights 81
3.2 Gas Factors 81
3.3 Angles and Energies of Experimental Points 89
3.4 Pion Production Ratios 108
3.5 Normalization Cross Sections, Angular Distribution 108
3.6 Normalization Cross Sections, Back Angles 109

4.1 ρ^+ and ρ^- , 142 MeV 117
4.2 ρ^+ and ρ^- , 180 MeV 117
4.3 ρ^+ and ρ^- , 220 MeV 118
4.4 ρ^+ and ρ^- , 256 MeV 118
4.5 r_1 and r_2 , 142 MeV 123
4.6 r_1 and r_2 , 180 MeV 123
4.7 r_1 and r_2 , 220 MeV 124
4.8 r_1 and r_2 , 256 MeV 124
4.9 R, 142 MeV 128
4.10 R, 180 MeV 128
4.11 R, 220 MeV 129
4.12 R, 256 MeV 129
4.13 142 MeV Cross Sections 137
4.14 180 MeV Cross Sections 137
4.15 220 MeV Cross Sections 138
4.16 256 MeV Cross Sections 138

List of Figures

1.1 π-nucleon Amplitudes at 180 MeV 5
1.2 ρ^+ and ρ^- From Previous Experiments 8
1.3 r_1 and r_2 From Previous Experiments 9
1.4 R From Previous Experiments 10
1.5 Momentum Transfer in Elastic Scattering 13
1.6 Momentum Transfer in Elastic Scattering 14
1.7 Gaussian Form Factor 17
1.8 Impulse Calculation, Cross Sections 19
1.9 Impulse Calculation, Ratios 20
1.10 ρ^+ , ρ^- , r_1 and r_2 With Various Radii, Simple Model 22
1.11 Diagram for Nucleon Correlations 26
1.12 r_1 and r_2 , Using Sum-of-Gaussian Form Factors 28
1.13 ρ^+ and ρ^- Using Sum-of-Gaussian Form Factors 29
1.14 Ratio Calculations, Kim, Krell, and Tiator 30
1.15 Ratio Calculations, Kim, Kim, and Landau 32
1.16 R Calculation 33
1.17 Cross Section Calculations, 180 MeV 35

2.1 EPICS Schematic 41
2.2 Pion Spectrum with no Muon Rejector 46
2.3 Over-Rejection 49
2.4 EURYDICE Placement 51
2.5 EURYDICE Geometry, Incident Particle 52
2.6 Complete EURYDICE Scattering Geometry 53
2.7 Gas Volume Definitions 57
2.8 Thin Target Scattering 58
2.9 Ray Tracing Comparison with Replay 60
2.10 Cylindrical Target Scattering, Single Scattering Angle 61
2.11 Nearside Scattering, 120° 62
2.12 Farside Scattering, 120° 63
2.13 Nearside Scattering, 173° 64
2.14 Farside Scattering, 173° 65
2.15 Ray Tracing Comparison with Replay 66
2.16 Angular Acceptance from Ray Tracing 67
2.17 EURYDICE Backscatter 70

2.18 EURYDICE Backscatter 71
2.19 Scattering Momentum Comparison 72

3.1 Angle Checks for Normalizations 78
3.2 Sample X_{target} 83
3.3 Y_{target} Shape With Angle 84
3.4 Y_{target} to Define Gas Volume 86
3.5 Acceptance Scan 88
3.6 D normalization runs at 146° 91
3.7 D run at 173° 92
3.8 Ratios for 'Flat' Spectra, High Counts 94
3.9 Ratios for 'Flat' Spectra, Low Counts 95
3.10 Good and Bad Background Subtraction 98
3.11 Background Under Elastic Peaks 99
3.12 Straight Line Background Example 100
3.13 Variation of ρ^+ With Peak Slice Width 101
3.14 r_1 By Two Methods 104
3.15 Several Calculations of ρD 105
3.16 Backangle ρD 106
3.17 $\pi^\pm$ production ratios 107
3.18 Normalization Cross Sections 109

4.1 ρ^+ and ρ^- 114
4.2 ρ^+ and ρ^- *vs* q^2 115
4.3 r_1 and r_2 121
4.4 r_1 and r_2 Comparison 122
4.5 The Superratio 126
4.6 Superratio-Calculation Comparison 127
4.7 Pion Scattering from ^{4}Helium and Tritium 131
4.8 142 MeV Cross Sections 133
4.9 180 MeV Cross Sections 134
4.10 220 MeV Cross Sections 135
4.11 Cross Section Calculations, Gibbs and Gibson 136

ELASTIC SCATTERING OF PIONS FROM TRITIUM AND ^{3}HE IN THE BACKWARD HEMISPHERE IN THE REGION OF THE $\Delta_{33}(1232)$ RESONANCE

by

Scott K. Matthews

ABSTRACT

Several experiments have measured nominally-charge-symmetric scattering of pions from tritium (^{3}H) and ^{3}He. These experiments have covered incident pion energies from 142 MeV to 295 MeV and scattering angles up to 110° in the laboratory. The results have been used to study charge-symmetry breaking and nuclear scattering systematics.

In the work I have extended these measurements to angles near 180° for pion energies of 142 MeV, 180 MeV, 220 MeV, and 256 MeV, which bracket the Δ_{33} pion-nucleon resonance. This is the most extensive set of πT and π^3He data in this kinematical region. It will allow tests of scattering theory of pion-nucleus interactions and charge-symmetry breaking in back-angle scattering, and, within the limits of these two theories, it may help improve our understanding of the structure of these nuclei.

Chapter 1

Physics

1.1 Introduction

Pion scattering from nuclear targets, which is dominated by the strong force, has been used to study nuclear structure for more than two decades. Recent experiments have shown that information on both nuclear structure and the charge symmetry (CS) of the basic π-nucleon and nucleon-nucleon interactions can be extracted by pion scattering from the isomirror nuclei ^{3}He and Tritium (T) [Nef90], [Pil91]. Complementary structure information can be extracted by electron scattering; however this probe can only measure the neutron distributions by spin-dependent interactions. Since the neutrons in T are paired, their resultant spin is zero, and the neutron radius of T cannot be measured in this way.

In the present experiments, we measure pion-scattering cross sections and cross section ratios at several energies near the Δ_{33} resonance, in the backward hemisphere. There is very little other ^{3}He and T data in this kinematical region, [Alb82], [Kal80].

1.2 The A = 3 System

There are two nuclei with three nucleons, Tritium (T) or ^{3}H, and ^{3}He. T has a single proton and two neutrons. The ground state predominantly has the neutrons paired with opposite spins. ^{3}He is the mirror nucleus of Tritium. It has two mainly spin-paired protons and a single neutron. There are no known excited states of either nucleus [Til87]. Their masses are almost identical; T is $\sim$ 20keV more massive than ^{3}He. The binding energies, however, are substantially different: 8.482 MeV for T, and 7.718 MeV for ^{3}He. This is a difference of 764 keV. Coulomb repulsion accounts for all but 40-80 keV of this [Gib91].

In the absence of the Coulomb interaction, and assuming that the nn and pp interactions are the same, we would expect ^{3}He and T to have exactly the same spatial distributions of nucleons. Since the np force is more attractive than

either the nn or pp force (the only bound two-nucleon state is Deuterium (D)), the 'odd' nucleon in each case (the proton in T and the neutron in ^{3}He) will feel more force, and so will have a smaller radius than the 'even' nucleons (the neutrons in T and the protons in ^{3}He); this difference is about 0.15 fm [Gib91]. Adding the Coulomb interaction increases the distance between the protons in ^{3}He. This means that the neutron in ^{3}He feels less force from the more-separated protons. Both the neutron and proton radii in ^{3}He should be expanded in this way, by around 0.02 to 0.04 fm [Gib91]. If the pp and nn nuclear forces are not equal, it is similar to adding an extra piece to the Coulomb interaction, and like effects should be seen.

Following [Gib91], the following definitions will be used: 'delta-even' (δ_e) for the difference between the neutron radius in T and the proton radius in ^{3}He, and 'delta-odd' (δ_o) for the difference between the neutron radius in ^{3}He and the proton radius in T. Because of the overall expansion in ^{3}He mentioned above, we expect δ_e to be negative, and δ_o to be positive.

An extensive review of the experimental and theoretical literature through 1987 is given by Tilley *et. al.* [Til87]. Gibbs and Gibson [Gib91] and the references cited therein give a good background for the topics covered in this work, including the basic scattering theory issues as well as historical perspective.

1.3 The Pion-Nucleon System

The pion is a meson with isospin I=1 , and spin S=0. It comes in three charges, corresponding to the three projections of isospin, I_z, 1, 0, and -1. These projections are called π^+, π^0 and π^-, respectively; they have charges +1, 0, and -1, and masses 139.57, 134.96, and 139.57 MeV/c^2. The nucleon has S = $\frac{1}{2}$ and $S_z = \pm\frac{1}{2}$, I = $\frac{1}{2}$ and $I_z = \pm\frac{1}{2}$. These isospin projections are called the proton (p) and the neutron (n), respectively; they have charges +1 and 0, and masses of 938.27 and 939.57 MeV/c^2.

The possible isospin combinations in π-nucleon scattering are I= $\frac{3}{2}$, $I_z = \pm(\frac{3}{2}, \frac{1}{2})$, and I = $\frac{1}{2}$, $I_z = \pm\frac{1}{2}$. The spin possibilities are S = $\frac{1}{2}$ and $S_z = \pm\frac{1}{2}$. The isospin can be regrouped using Clebsch-Gordan coefficients. If we designate a state with I = $\frac{3}{2}$ and $I_z = \frac{1}{2}$, for example, as $|\frac{3}{2}, \frac{1}{2}>$, and use similar notation for the other combinations, then we can rewrite the various scattering combinations as

$$\pi^+ p = |\tfrac{3}{2}, \tfrac{3}{2}>, \tag{1.1}$$

$$\pi^+ n = \sqrt{\frac{1}{3}}|\tfrac{3}{2}, \tfrac{1}{2}> + \sqrt{\frac{2}{3}}|\tfrac{1}{2}, \tfrac{1}{2}>, \tag{1.2}$$

$$\pi^0 p = \sqrt{\frac{2}{3}}|\tfrac{3}{2}, \tfrac{1}{2}> - \sqrt{\frac{1}{3}}|\tfrac{1}{2}, \tfrac{1}{2}>, \tag{1.3}$$

$$\pi^0 n = \sqrt{\frac{2}{3}}|\tfrac{3}{2}, -\tfrac{1}{2}> + \sqrt{\frac{1}{3}}|\tfrac{1}{2}, -\tfrac{1}{2}>, \tag{1.4}$$

$$\pi^- p = \sqrt{\frac{1}{3}} | \tfrac{3}{2}, -\tfrac{1}{2} > - \sqrt{\frac{2}{3}} | \tfrac{1}{2}, -\tfrac{1}{2} >, \quad (1.5)$$

$$\pi^- n = | \tfrac{3}{2}, -\tfrac{3}{2} >. \quad (1.6)$$

There is an experimentally observed resonance in π-nucleon scattering for incoming pions with energy of $\sim$ 180 MeV with the nucleon at rest. This resonance, called the 'Delta Resonance' (Δ_{33}), occurs when the spatial-angular momentum quantum number ℓ is 1, the total angular momentum quantum number J is $\frac{3}{2}$, and the total isospin I is $\frac{3}{2}$.

Consider elastic π^+ n scattering at 180 MeV. The scattering amplitude will contain a term that looks like

$$< \pi^+ \; n \; |M| \; \pi^+ \; n >, \quad (1.7)$$

which can be rewritten as

$$\left(\sqrt{\frac{1}{3}} < \tfrac{3}{2}, \tfrac{1}{2} | + \sqrt{\frac{2}{3}} < \tfrac{1}{2}, \tfrac{1}{2} | \right) (M) \left(\sqrt{\frac{1}{3}} | \tfrac{3}{2}, \tfrac{1}{2} > + \sqrt{\frac{2}{3}} | \tfrac{1}{2}, \tfrac{1}{2} > \right),$$

where M is the transition operator. The amplitude does not depend on the I_z value if we assume that CS holds for π-nucleon interactions. Assuming the conservation of I in the π-nucleon interactions, and that the transition does not depend on I_z, so the I_z component can be suppressed, we can rewrite this as

$$\frac{1}{3} < \tfrac{3}{2} \; |M| \; \tfrac{3}{2} > + \frac{2}{3} < \tfrac{1}{2} \; |M| \; \tfrac{1}{2} > \equiv \frac{1}{3} M_3 + \frac{2}{3} M_1.$$

On resonance, that is. where the incoming pion kinetic energy is 180 MeV, and $M_3 \gg M_1$. this is just $\frac{1}{3} M_3$.

With these assumptions, after forming matrix elements like Eq. 1.7 for $\pi^+ p$, $\pi^- p$, *etc.*, we can write down the following relationships for the scattering cross sections, either total or differential, which are proportional to the square of the amplitudes:

$$\begin{aligned} \sigma(\pi^+ \; p) &= 9\sigma(\pi^+ \; n), \\ \sigma(\pi^- n) &= 9\sigma(\pi^- p), \\ \sigma(\pi^+ \; p) &= \sigma(\pi^- n), \\ \sigma(\pi^+ \; n) &= \sigma(\pi^- p). \end{aligned}$$

If we assume that a system that has total spin = $\frac{1}{2}$ is invariant under rotations and parity reversals, then it can be shown [Tay72, Chap. 6] that the scattering amplitude can be written as

$$A(\theta, E) = f(\theta, E) + ig(\theta, E) \hat{\mathbf{n}} \cdot \sigma$$

where f and g are called the *non-spin-flip* and ***spin-flip*** amplitudes, respectively. They are the amplitudes for scattering where the third component of the spin

of the nucleon is 'flipped' (has its sign changed) or not 'flipped' during the interaction. θ is the scattering angle, E is the total energy, $\hat{\mathbf{n}}$ is a unit vector perpendicular to the scattering plane, and σ is the Pauli representation of the spin, that is, $\mathbf{S} = \frac{1}{2}\sigma$. The differential cross section is the magnitude of this amplitude,

$$\frac{d\sigma}{d\Omega} = \mid f \mid^2 + \mid g \mid^2, \tag{1.8}$$

in the case where the target is not polarized and the scattering asymmetry is not measured. Near the Δ_{33}-resonance energy, the interaction is dominated by the $\ell = 1$partial wave; the spin-flip amplitude has a sine dependence and the non-spin-flip amplitude has a cosine dependence.

Figure 1.1 shows the basic amplitudes for $\pi^{\pm}$ p, at the pion-resonance energy of 180 MeV, from the VPI phase-shift analysis [Arn85]. Except at far-forward angles, most of the amplitude is in the imaginary parts. The sine and cosine shapes of the spin-flip and non-spin-flip parts are obvious. The $\pi^- p$ amplitudes are $\sim \frac{1}{3}$ of the $\pi^+ p$, as predicted. There will be a dip at 90°, the 'non-spin-flip dip' (NSF dip), in any amplitudes that depend primarily on the non-spin-flip part, because of the cosine dependence.

1.4 Charge Symmetry

Charge Symmetry (CS) is defined as equality under the operation of charge conjugation. In the case of πT and π^3He scattering, charge conjugation changes π^+ into $\pi^-$and *vice versa*, and also changes T and ^{3}He into each other (by reversing the protons and the neutrons). Therefore, if charge symmetry were universal, we would expect π^+T to be the same as π^{-3}He, and π^-T to be the same as π^{+3}He. CS can be broken in four ways in this system. The first charge-symmetry breaking (CSB) effect is Coulomb scattering. The Coulomb force is not charge symmetric; thus the different charge combinations of pions and nucleons are important. In general, Coulomb scattering is of the order $1/137^2$ less than the strong force scattering, so this should be a small effect. However, in the region of the NSF dip, some of the primary amplitudes are going through zero (see Fig. 1.1). We might expect that Coulomb interference could be important there.

The second CSB effect is also due to the Coulomb force. Coulomb repulsion pushes the protons in ^{3}He apart, forcing the neutron radius in ^{3}He to increase as well. Because of this ^{3}He is larger than T, and so the form factor of ^{3}He will fall off more quickly with momentum transfer than will that of T(see Sec. 1.6.2). In general, the ^{3}He cross sections will be less than the T cross sections in nominally charge-symmetric situations. For instance, because of this size difference, we expect

$$\sigma(\pi^+\mathrm{T}) > \sigma(\pi^{-3}\mathrm{He}).$$

The third CSB effect is due to any difference in the nn force with respect to the pp force. For example, if the pp force is greater than the nn force after

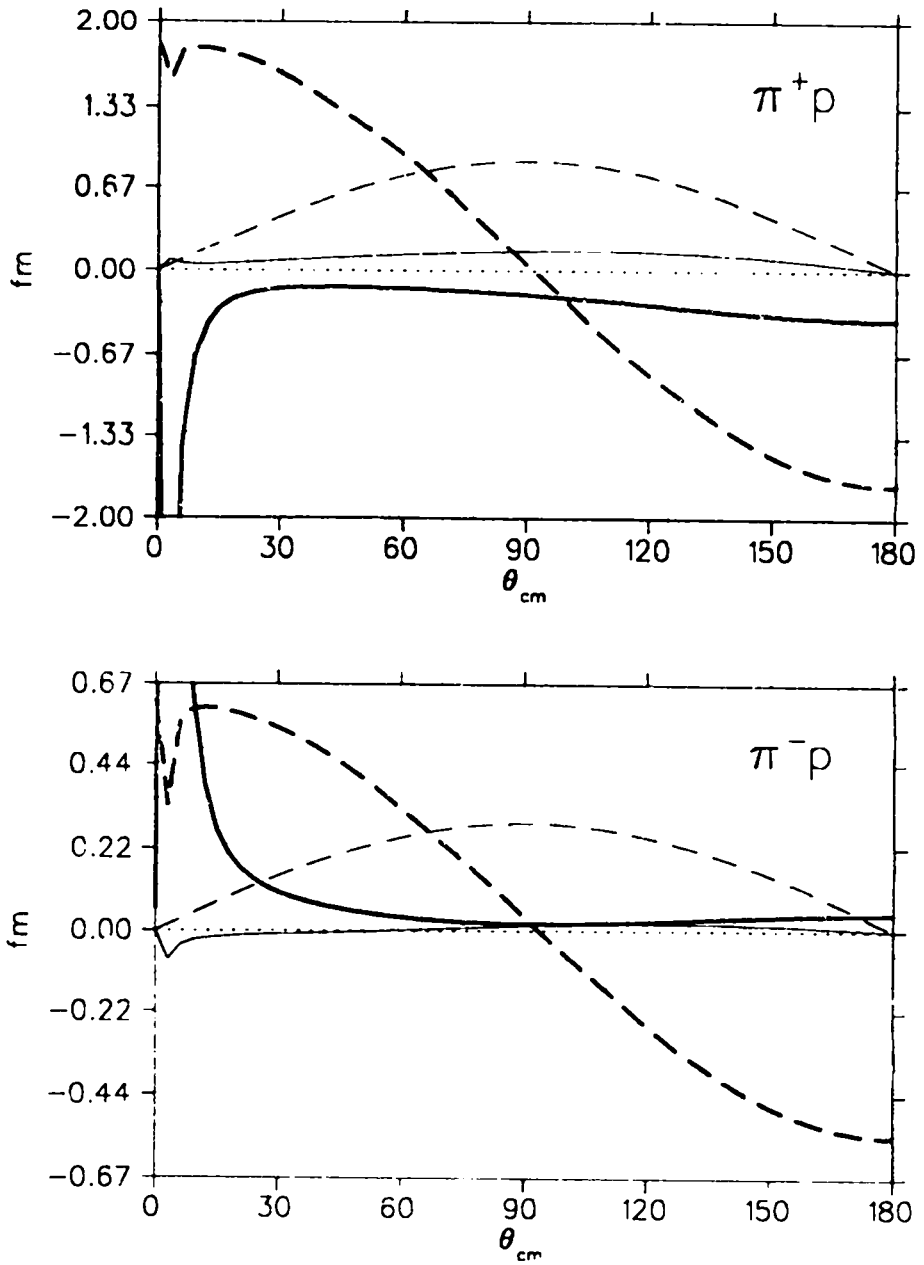

Figure 1.1: π-nucleon scattering amplitudes, for 180 MeV pions and stationary nucleons (in the lab frame), as a function of scattering angle in the π-nucleon center of mass, from the VPI phase shift analysis [Arn85]. The bold lines are the non-spin-flip amplitudes, the lighter lines are spin-flip amplitudes. The real parts of the amplitudes are shown solid, the imaginary parts dashed. The dotted lines show zero amplitude, for reference.

the electromagnetic interaction has been accounted for, then the proton radius will be increased in ^{3}He over the neutron radius in T, beyond the increase due to Coulomb repulsion. This is an example of Nuclear-Charge-Symmetry Breaking (NCSB).

The final CSB effect is a difference in the strong πN amplitudes as a function of isospin projection. A good measure of this is given by pion scattering from Deuterium. Recent measurements by Smith *et. al.* [Smi88] found an overall asymmetry of $\sim -1.5\%$ for π^+D and π^-D scattering at the resonance energy in the backward hemisphere, independent of scattering angle. Neglecting Coulomb effects, this scattering should be charge symmetric; if the reported asymmetry is correct, we can expect it to show up in the current results as well.

1.5 Ratios

Several scattering ratios have been defined by Nefkens *et. al.* [Nef90] that help to illuminate different parts of the pion interactions with $A = 3$ targets, and which also give some evidence for NCSB [Nef90]. They are:

$$\begin{aligned}
\rho^+ &= d\sigma(\pi^+\mathrm{T})/d\sigma(\pi^{+3}\mathrm{He}) \ , \\
\rho^- &= d\sigma(\pi^-\mathrm{T})/d\sigma(\pi^{-3}\mathrm{He}) \ , \\
r_1 &= d\sigma(\pi^+\mathrm{T})/d\sigma(\pi^{-3}\mathrm{He}) \ , \\
r_2 &= d\sigma(\pi^-\mathrm{T})/d\sigma(\pi^{+3}\mathrm{He}) \ , \textit{and} \\
R &= r_1 \times r_2 \ = \rho^+ \ \times \rho^- \ .
\end{aligned}$$

A brief discussion of each ratio is given below.

ρ^+ ... π^+T is in the numerator. At the resonance energy, scattering from the proton will dominate; both spin-flip and non-spin-flip scattering are possible. The denominator, π^{+3}He, is dominated by π^+ on the spin-paired protons, and so predominantly non-spin-flip scattering. Near the NSF dip, at 78° in the π-nucleus center of mass (90° in the π-nucleon center of mass), the non-spin-flip amplitude goes through zero, so most of the scattering is spin-flip. The denominator reflects this dip, since it is primarily NSF, but the numerator can still experience spin-flip on the single proton. Therefore, there is a peak in ρ^+ around 78°. As the scattering angle approaches back angles, the spin-flip amplitude goes to zero, and the non-spin-flip amplitude dominates for single scattering. This means that the denominator, which has twice as many protons as the numerator, is larger, and ρ^+ should decrease at large angles, in a single-scattering picture.

ρ^- ... The systematics are the inverse of those for ρ^+ . Because $\pi^- n$ is predominant, there is a dip in the NSF dip region where ρ^+ has a bump, and the ratio should rise at back angles for single scattering, because the two

resonance interactions in the numerator will dominate the single resonance interaction in the denominator as the spin-flip term goes to zero.

r_1 ... The numerator, π^{+3}He , and the denominator, π^-T , are isomirror interactions. Therefore, if CS were strictly observed, r_1 would equal 1.0.

The Coulomb interaction is not charge symmetric. There is twice as much Coulomb scattering in the denominator as in the numerator, because there are twice as many charged nucleons in ^{3}He as there are in T, and so both the pure Coulomb scattering and the Coulomb interference is not the same for numerator and denominator, (see Sec. 1.6.1). Furthermore, the protons in ^{3}He will feel a mutual repulsion, so they will be farther apart than the neutrons in T. This repulsion is reflected in an increased separation, and therefore a decreased form factor, decreasing the cross section in the denominator. Finally, the effect of the Coulomb-nuclear interference depends on the relative phase of the nuclear and Coulomb amplitudes.

The Coulomb-scattering effects are small, so we expect that the the difference in form factors to dominate and r_1 should be greater than 1.0. Generally, r_1 emphasizes scattering from the *unpaired* nucleons, p in T and n in ^{3}He, at the resonance energy.

r_2 ... This ratio is also nominally charge symmetric, and the decrease of the form factor of ^{3}He in the numerator should cause r_2 to be greater than 1.0, as was the case for r_1 . Since r_2 emphasizes the paired nucleons at the resonance energy, it will be primarily non-spin-flip scattering. At the NSF dip, since only spin-flip is left, it will be a ratio of the 'non-resonance interactions', that is $\pi^- p \,/\pi^+ n$.

R... The Superratio can be formed as the product or r_1 and r_2 , and equivalently of ρ^+ and ρ^- . It will have the same first-order corrections for Coulomb effects in both the numerator and the denominator, so it is less sensitive to Coulomb than the other ratios. If CS is universally true, R is 1.0.

These ratios have been measured in three previous experiments, for a variety of energies in the forward hemisphere [Nef90] [Pil91] [Pil92] [Ber91]; the results are shown in the following figures.

The bump at 78° that corresponds to the NSF dip is obvious in ρ^+ , ρ^- , r_2 and R, for 142 MeV and 180 MeV incident pions. The larger error bars on r_1 and r_2 are due to the fact that the normalizations do not cancel there (see Chapter 3).

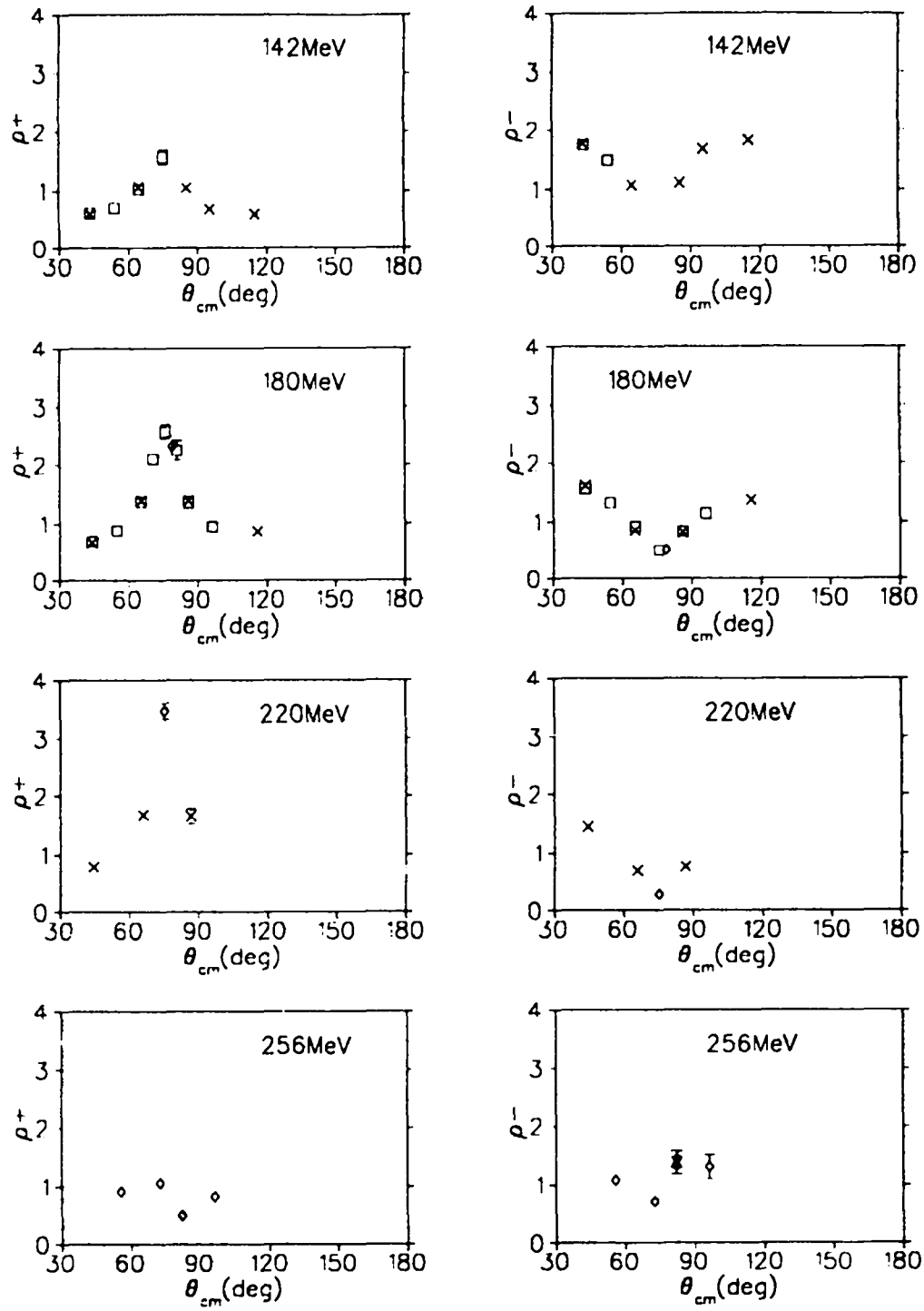

Figure 1.2: ρ^+ and ρ^- from previous LAMPF experiments. □ Exp. 546 [Nef90], × Exp. 905 [Pil91], ◇ Exp. 1032 [Pil92] and [Ber91]. The structure at $\sim 78°$ corresponds to the NSF dip.

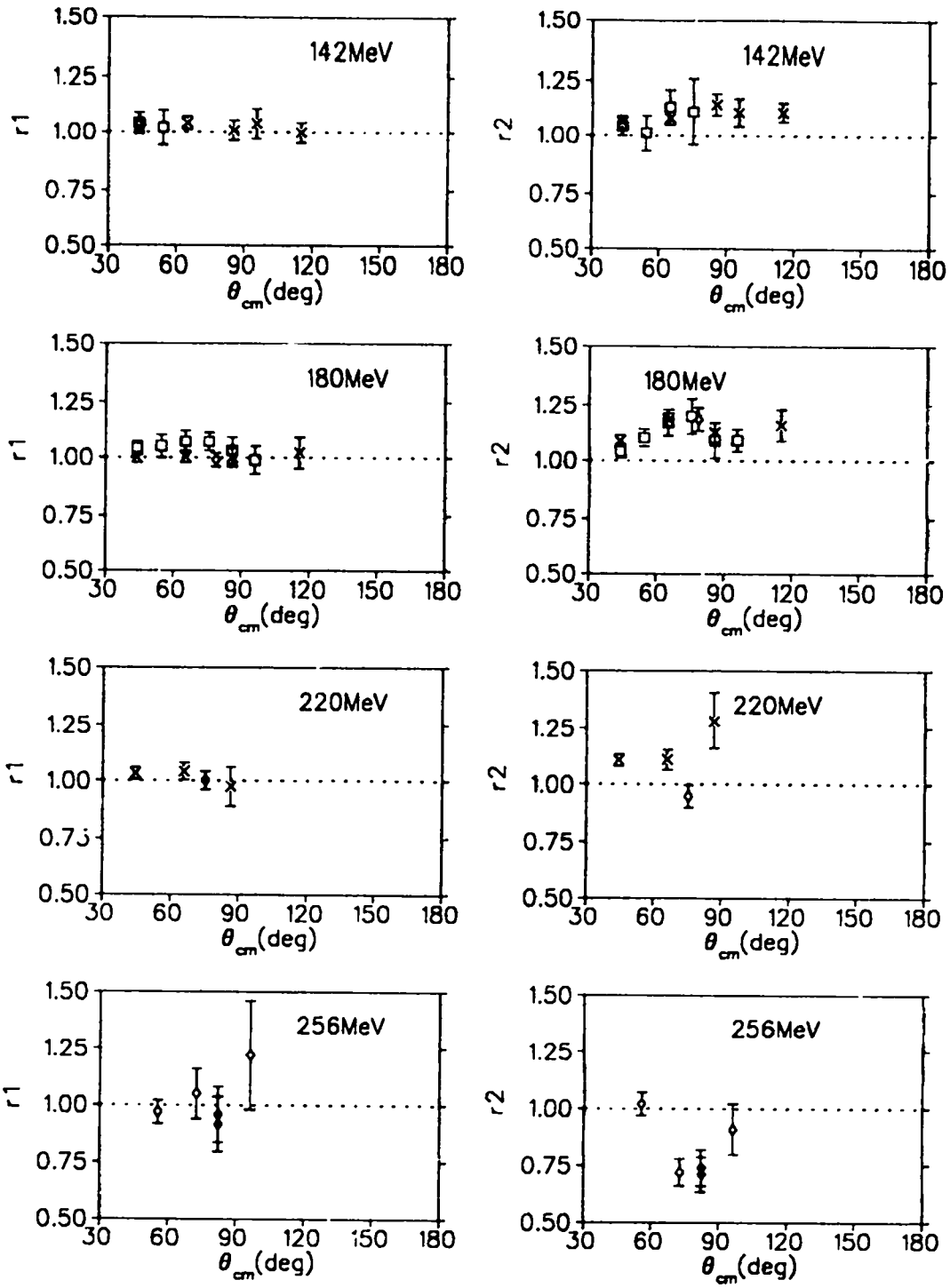

Figure 1.3: r_1 and r_2 from previous LAMPF experiments. □ Exp. 546 [Nef90], × Exp. 905 [Pil91], ◇ Exp. 1032 [Pil92] and [Ber91].

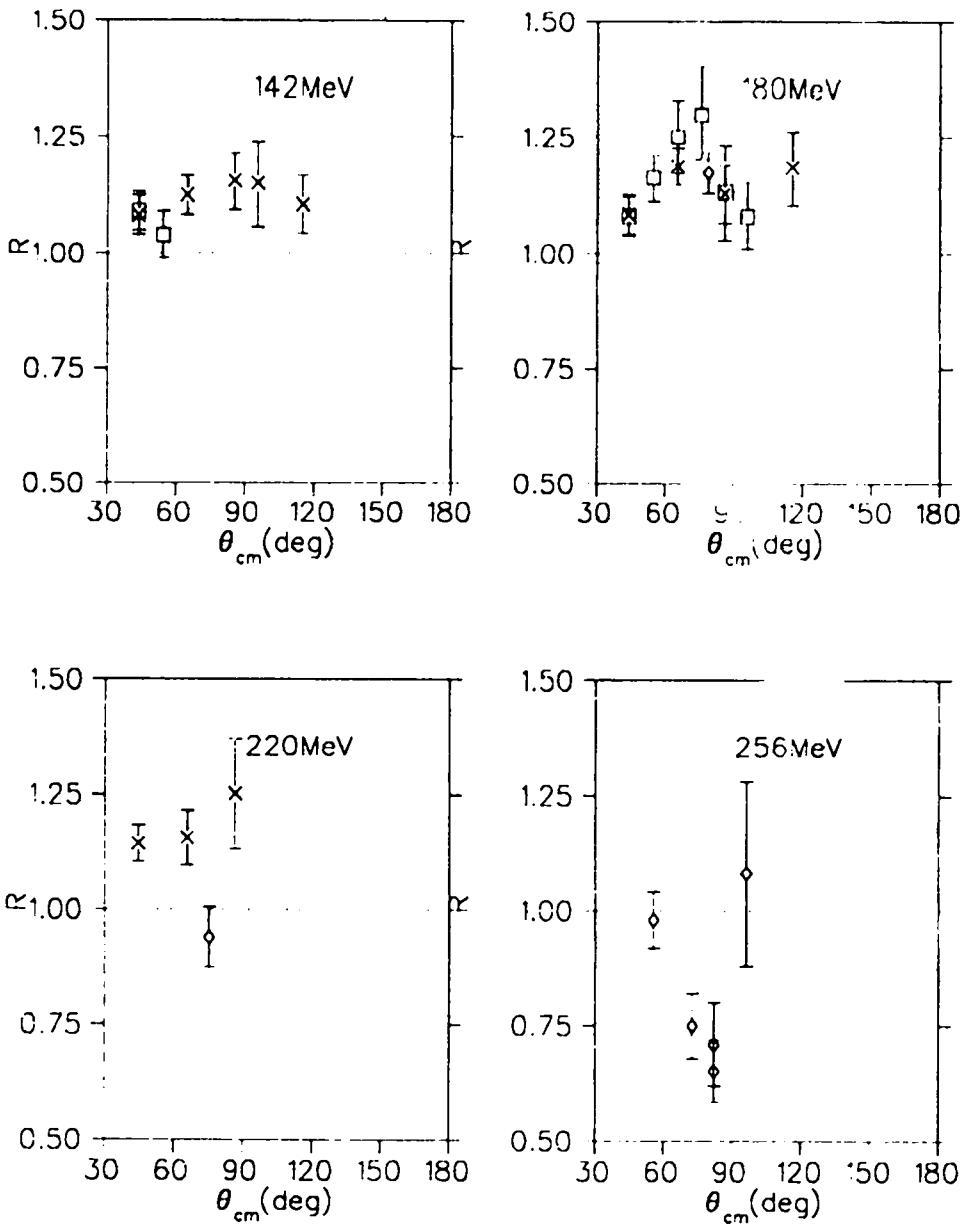

Figure 1.4: R from previous LAMPF experiments. □ Exp. 546 [Nef90], × Exp. 905 [Pil91], ◇ Exp. 1032 [Pil92] and [Ber91].

1.6 Elastic Scattering

Elastic scattering is a scattering reaction that leaves both participants in the same states they occupied before the collision. Although intermediate states that are not the same as the final states can be included in a multiple-scattering calculation, very often it is assumed that both participants remain in their original states throughout the entire process. In single scattering, this is the only possibility. Since there is no rearrangement, this is a good way to study some aspects of nuclear structure. π-nucleus scattering is a combination of two interactions. Because both the pions and the nucleons have charge, there is the Coulomb force. The pions and the nucleons also interact through the strong force, and the proper description of the interaction includes both forces.

1.6.1 Coulomb Scattering

Coulomb scattering is a small part of the interaction because of the coupling constant $\alpha = \frac{1}{137}$, compared to ~ 1.0 for the strong force. The Rutherford formula for Coulomb scattering is

$$d\sigma/d\Omega = \frac{z^2\mu^2}{4p^2\sin^4(\theta/2)}$$

where z is the charge of the nucleus , μ is the reduced mass, p is the center-of-mass momentum and θ is the scattering angle. The fourth power of the sine in the denominator means that the cross section is very large at small angles, and drops off rapidly as the angle increases. In a potential-interaction description of π-nucleus scattering, the Coulomb interaction can be included as a separate term in the scattering amplitude.

$$f = f_C + f_N e^{-i2\phi}$$

where f_N refers to the strong-force amplitude, and 2ϕ describes the phase between the two [Tay72] [Bin78].

Since the cross section is the square of the amplitude, we can write

$$\frac{d\sigma}{d\Omega} = |f_N|^2\left[1 + \frac{|f_C|^2}{|f_N|^2} + 2\frac{|f_C|}{|f_N|}\frac{Re\ f_N}{|f_N|}\left(\cos(2\phi) + \frac{Im\ f_N}{Re\ f_N}\sin(2\phi)\right)\right].$$

The last two terms in the square brackets are the fractional change due to the Coulomb interaction. Especially at back angles, the Coulomb contribution should be small, because of the factors of f_C/f_N. However, in regions where the strong amplitudes are small, such as at the NSF dip, the Coulomb force may become important. Whether it can be neglected must be investigated in each case.

1.6.2 Nuclear Scattering

Many scattering quantities are reported in terms of the four momentum transfer

$$q \equiv (E_f, \mathbf{p}_f) - (E_i, \mathbf{p}_i),$$

where the subscripts refer to the final and initial quantities, that is, for the outgoing and incoming pion. For elastic scattering, the energy is conserved, and

$$q^2 = q^\mu q_\mu = -\mathbf{q} \cdot \mathbf{q}. \equiv t$$

The units used throughout are inverse-fermis squared (fm^{-2}).

An interaction is limited kinematically by the amount of momentum that can be transferred from the projectile to the target. In elastic scattering, we consider the nucleus as a single particle. Momentum and energy must be conserved with this particle and the projectile in any scattering interaction, so for scattering at a given angle the momentum transfer is found from π-nucleus kinematics. However, if we assume that the scattering involved just a single interaction of a pion with one nucleon (single scattering), then the total momentum transfer must come from that interaction. Figure 1.5 and Figure 1.6 show calculations of the momentum transfer for scattering from tritons and nucleons. Four curves are calculated for each energy that is covered by these experiments. The solid curve is for scattering from the Triton. The dashed curve is scattering from an at-rest nucleon. The two dotted curves are for scattering from nucleons with non-zero nuclear momenta. In each plot, the upper dotted curve is for nucleons with nuclear momentum of 200 MeV/c, and the lower dotted curve is for nuclear momentum of 100 MeV/c. For every energy except 295 MeV, it is possible to get the required momentum transfer for scattering out to 180° from single scattering, although for the largest angles, only the tail of the nuclear-momentum distribution will suffice. This means that the probability for single scattering decreases as a function of the momentum transfer. The curves show that single-scattering is important throughout the entire angular range at 142 MeV, and that its importance decreases as the incident energy increases. At 295 MeV, it will be impossible at the largest angles for all but the highest-momentum nucleons. We should be able to have a very large component of single scattering at least to the angle of the NSF dip, since at that point for 180 MeV pions there is good overlap between the π-nucleus momentum transfer and the momentum transfer from 100 MeV/c nucleons, as shown in Fig. 1.5.

1.6.3 Pion-Nucleus Scattering

For a π-nucleus interaction described by a Hamiltonian

$$\begin{aligned} H &= H_0 + V \\ &= H_N + K_\pi + \sum_{i=1}^{A} v_i(\mathbf{r} - \mathbf{r_i}), \end{aligned}$$

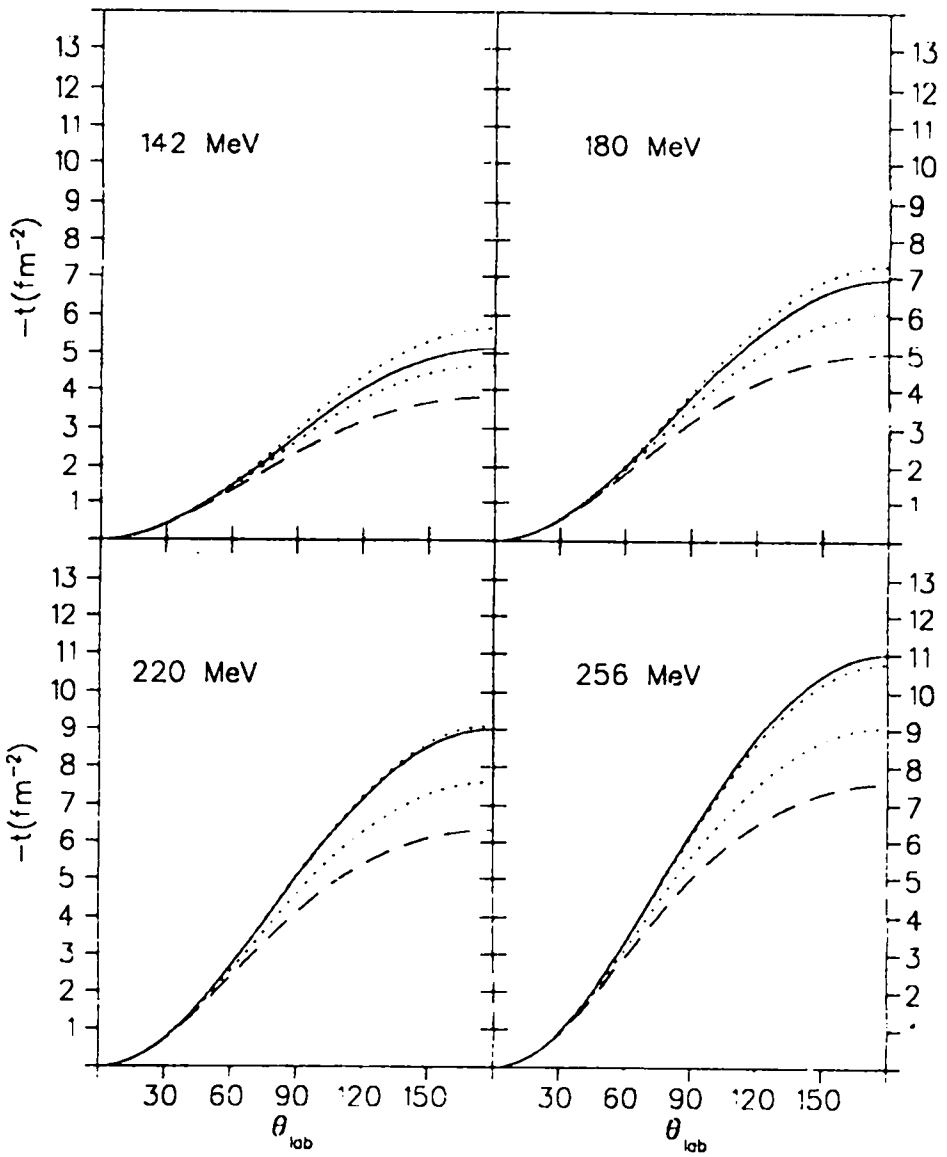

Figure 1.5: Momentum transfer as a function of center-of-mass scattering angle for the π-nucleon and the π-nucleus systems, for four incident-pion energies. In each figure, the solid line is momentum transfer to the nucleus, and the dashed line is momentum transfer from a free nucleon at the same incident pion energy and laboratory scattering angle. The dotted lines are the maximum possible momentum transfer from moving nucleons; with nucleon momentum of 200 MeV/c for the top line in each case, and 100 MeV/c for the bottom dotted line.

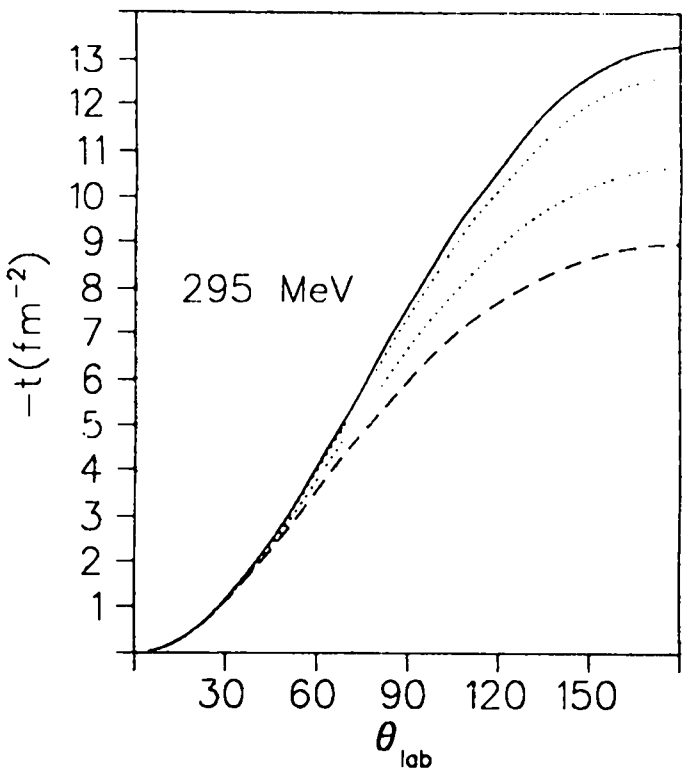

Figure 1.6: Momentum transfer as a function of center-of-mass scattering angle for the π-nucleon and the π-nucleus systems, for an incident-pion energy of 295 MeV. The different lines are described in Fig. 1.5.

where H_N is the nuclear Hamiltonian, A is the number of nucleons in the nucleus, K_π is the pion kinetic energy, and v_i is the interaction between the pion at coordinate $\mathbf{r}$, and the nucleon at $\mathbf{r_i}$, we can write an equation for the T matrix

$$T = V + VGT = \sum_{i=1}^{A} v_i + \sum_{i=1}^{A} v_i GT.$$

This background material is from [Eis80, Chap. 3,4]. The scattering amplitude is

$$< \mathbf{k}' \, \mathbf{p}' \, \alpha' \, |T| \, \mathbf{k} \, \mathbf{p} \, \alpha >, \tag{1.9}$$

where $\mathbf{k}', \mathbf{k}$ and $\mathbf{p}', \mathbf{p}$ are the final and initial momenta of the pion and nucleus, respectively, and α', α refer to the final and initial total spin and isospin. G is the Green function or propagator for the pion in the nuclear medium

$$G = \frac{1}{E - H_N - K_\pi + i\eta},$$

where E is the total energy and η is taken to zero after the integral to determine the amplitude is completed. After some algebra, we can write

$$T_i \equiv t_i + t_i G \sum_{j \neq i}^{A} T_j, \tag{1.10}$$

$$T = \sum_{i=1}^{A} T_i, \tag{1.11}$$

$$t_i = v_i + v_i G t_i. \tag{1.12}$$

t_i is the amplitude for scattering from a single nucleon in the nuclear medium. In the case where the nuclear Hamiltonian can be neglected with respect to the pion kinetic energy,

$$t_i \sim t_i^{free}, \tag{1.13}$$

is the amplitude for scattering from a free nucleon. Note that $t_i = t_i(E)$, where E is the total interaction energy, found in the propagator.

In elastic scattering, the initial and final nuclear states will be the ground state. We expect the first part of the expansion for T_i to be greater than the terms in the summation $t_i G \sum_{j \neq i}^{A} T_j$ because the latter contains products of amplitudes. Retaining only the initial term, 1.9 can be rewritten as

$$\sum_{i=1}^{A} < 0 \, |< \mathbf{k}' \, \mathbf{p}_i' \, \alpha' \, |t_i| \, \mathbf{k} \, \mathbf{p}_i \, \alpha >| \, 0 >$$

$$= \sum_{i=1}^{A} \int d\mathbf{p_1} \ldots d\mathbf{p_i}, d\mathbf{p_i'} \ldots d\mathbf{p_A}$$

$$\times \Phi_0^\dagger(\mathbf{p_1} \ldots \mathbf{p_i'} \ldots \mathbf{p_A}) t_i^\sigma(\mathbf{k}', \mathbf{k}, \mathbf{p}, E) \delta(\mathbf{p_i'} + \mathbf{k}' - \mathbf{p} - \mathbf{k}) \Phi_0(\mathbf{p_1} \ldots \mathbf{p_i'} \ldots \mathbf{p_A}).$$

The matrix $< \mathbf{k}'\ \mathbf{p}_i'\ \alpha'\ |t_i|\ \mathbf{k}\ \mathbf{p}_i\ \alpha >$ has been replaced by a number that depends on the interaction energy and a delta function that conserves momentum among the pion and struck nucleon. Φ_0 refers to the nuclear ground state. The delta function serves to replace $\mathbf{p}_i'$ with $\mathbf{p}_i - (\mathbf{k}' - \mathbf{k}) \equiv \mathbf{p}_i - \mathbf{q}$.

If we ignore the motion of the struck nucleon, that is take $\mathbf{p}_i = \mathbf{p}_i' = 0$ when considering the amplitude t_i, we have the fixed-scatterer approximation. The amplitude becomes

$$\sum_{\alpha,i} t_{\alpha,i}(\mathbf{k}'\ \mathbf{k}\ E) \int d\mathbf{p}_1 \ldots d\mathbf{p}_A \Phi_0^{\alpha\dagger}(\mathbf{p}_1 \ldots \mathbf{p}_i - \mathbf{q} \ldots \mathbf{p}_A)\Phi_0^{\alpha}(\mathbf{p}_1 \ldots \mathbf{p}_i \ldots \mathbf{p}_A).$$

The ground states have been replaced by functions that refer to the proton and neutron ground states, taken separately. α refers to the nucleon type, and i is an index within this type, such as the first neutron, the second neutron, *etc.* . This removes direct isospin dependence in favor of describing the neutrons and protons individually. We can rewrite the integral as

$$F_\alpha(\mathbf{q}) \equiv \int d\mathbf{r} e^{i\mathbf{q}\cdot\mathbf{r}} \rho^\alpha(\mathbf{r}), \tag{1.14}$$

and the amplitude becomes

$$\sum_{i,\alpha} t_{i,\alpha}(\mathbf{q}, E) F_\alpha(\mathbf{q}). \tag{1.15}$$

The form factor is the Fourier transform of the nuclear density, the ratio between scattering from an extended object, and scattering from a point. The electromagnetic form factor for T are reported in [Jus85],[Bec82] and [Col65], and for ^{3}He in [McC77], as well as others. The charge form factor measured this way, F_{ch}, reflects the spatial distribution of protons in the nuclei, that is it is similar to the body form factor.

The form factors are given as functions of the 4-momentum transfer, squared, q^2. Figure 1.7 shows the ^{3}He charge form factor measured by [McC77]. If we assume a gaussian shape for the nuclear density, then

$$F_{ch} = e^{-q^2 R^2/6} \tag{1.16}$$

where R is the nuclear radius. As the figure shows, an effective radius, $R_{eff} = 1.73$ fm, gives a good match to the data in the region of the current experiments, up to about $-t \equiv q^2 = 8\text{fm}^{-2}$. $R_{eff} = 1.60$ fm does a similarly good job for the T data, which is not shown.

1.6.4 A Simple Calculation

With the approximation in 1.13, we can use the π-nucleon amplitudes shown in Fig. 1.1 in Eq. 1.15 to get the scattering amplitudes. However, α refers to the proton and neutron, so we need an expression for the neutron form

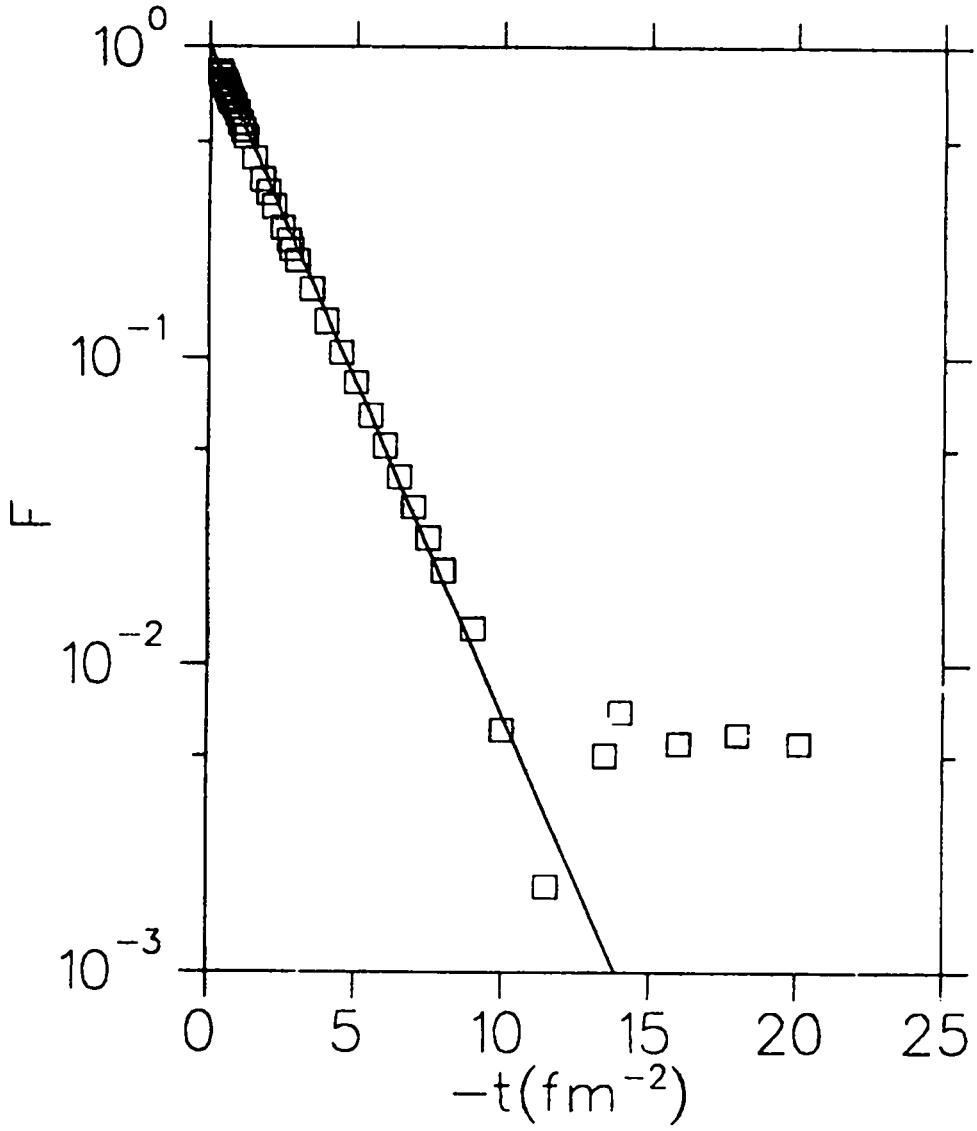

Figure 1.7: Form factors for e^3He scattering, and a gaussian form factor calculated with $R = 1.73$ fm.

factor. We expect the neutrons and protons to have similar distributions. In particular, under charge symmetry, the neutron in ^{3}He should have exactly the same distribution as the proton in T; likewise, the protons in ^{3}He and the neutrons in T.

Gibbs and Gibson, see Sec. 1.7, suggest that proton repulsion in ^{3}He leads to an increase in the proton radius of ^{3}He over the neutron radius of T of 0.030 fm while the neutron radius of ^{3}He is greater than the proton radius of T by 0.035 fm. In a gaussian form factor such as in Eq. 1.16 we can just change the value of R_{eff} to accommodate these radius differences. In the following calculation, the charge form factors measured in electron scattering are used at each value of q^2 for pion scattering from the protons. Expanding R^2_{eff}

$$R^2_{eff} = (R_p + \delta)^2 = R_p^2 + 2R_p\delta + \cdots,$$

where R_p is the proton-distribution radius and δ is the small change to get the neutron-distribution radius. Then, we can multiply the measured proton form factors by $e^{-2q^2R_p\delta/6}$ to get the neutron form factors. In doing this we assume the neutron distribution has the same basic shape as that of the protons, but that the neutron distributions' radius is different.

In π-nucleus elastic scattering, we cannot have spin-flip scattering from the spin-paired nucleons, protons in ^{3}He and neutrons in T, because the Pauli principle forbids them to have the same spin in the ground state, and there are no excited states to occupy. We can write out the amplitude for the fixed-scatterer approximation using the free nucleon amplitudes as

$$\begin{aligned}
A(\pi^+\mathrm{T}) &= F_{pT}\,[f(\pi^+p) + g(\pi^+p)] + 2F_{nT}\,f(\pi^+n), \\
A(\pi^+{}^3\mathrm{He}) &= 2F_{p^3He}\,f(\pi^+p) + F_{n^3He}\,[f(\pi^+n) + g(\pi^+n)], \\
A(\pi^-\mathrm{T}) &= F_{pT}\,[f(\pi^-p) + g(\pi^-p)] + 2F_{nT}\,f(\pi^-n), \\
A(\pi^-{}^3\mathrm{He}) &= 2F_{p^3He}\,f(\pi^-p) + F_{n^3He}\,[f(\pi^-n) + g(\pi^-n)],
\end{aligned}$$

where the form factors are written as, for example, F_{pT} , the form factor for protons in T.

Fig. 1.8 is an example of this calculation, which will be called the Simple Model henceforth, for 180 MeV pions. The match is good up until the vicinity of the NSF dip. From the momentum transfer calculations, we would only expect the fixed-scatterer, that is zero-momentum nucleon, approximation to be good to 60° — 70° in the center of mass, and the dip occurs at about 78°.

Fig. 1.9 shows the same calculation, this time for the ratios ρ^+ , ρ^- , r_1 and r_2 . The effect of the dip is very prominent for ρ^+ and ρ^- . For example in ρ^+ , the numerator is π^+T, at resonance energies this is primarily π^+p , on the *unpaired* nucleon, so spin-flip can occur. In the denominator, the resonance scattering is from *paired* protons, which can not undergo spin-flip scattering. So, as the angle approaches the value for the NSF dip, the denominator goes as the disappearing non-spin-flip amplitude, while the numerator goes with the

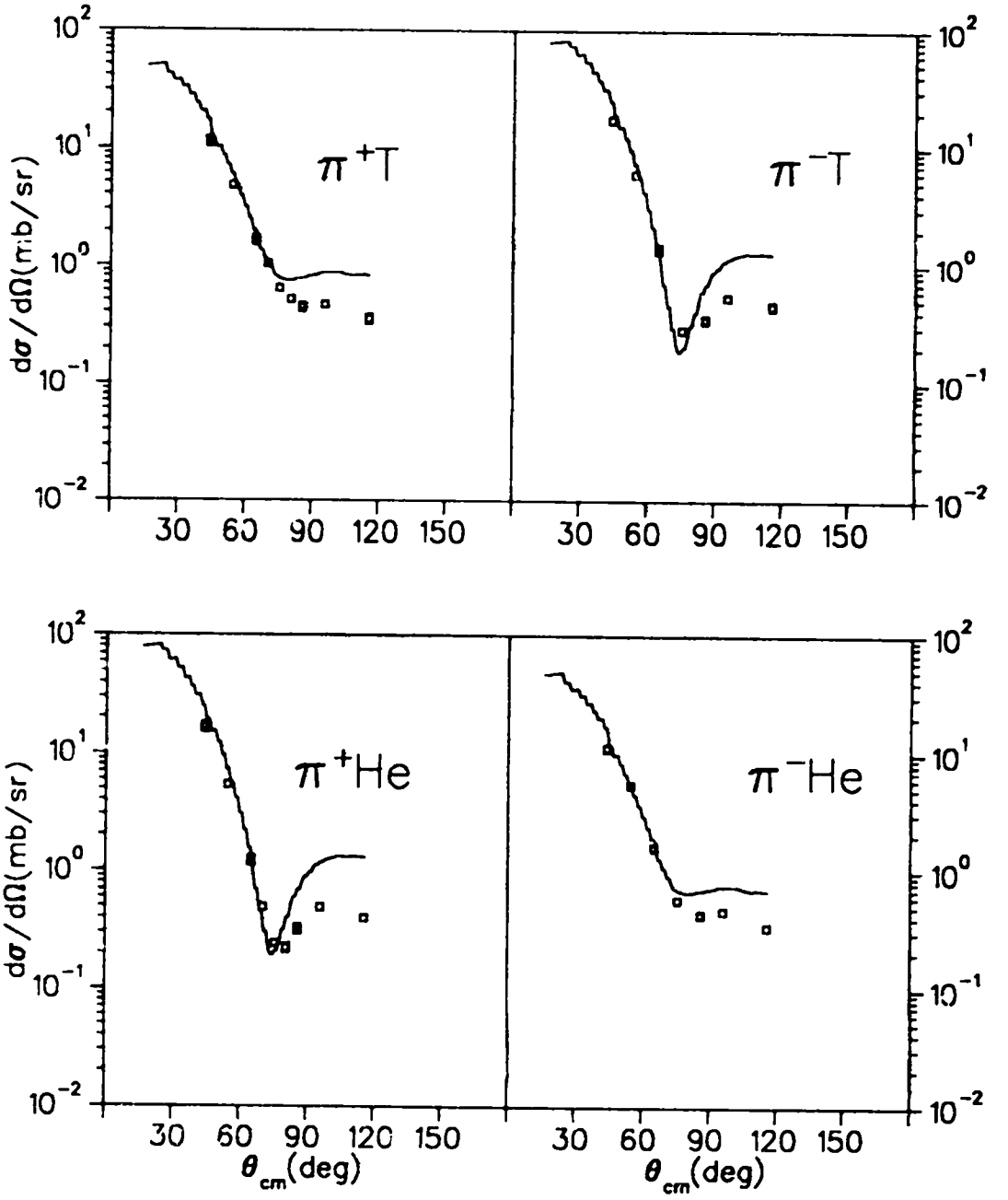

Figure 1.8: A fixed-scatterer impulse calculation of the 180 MeV cross sections from previous experiments [Nef90] [Pil91].

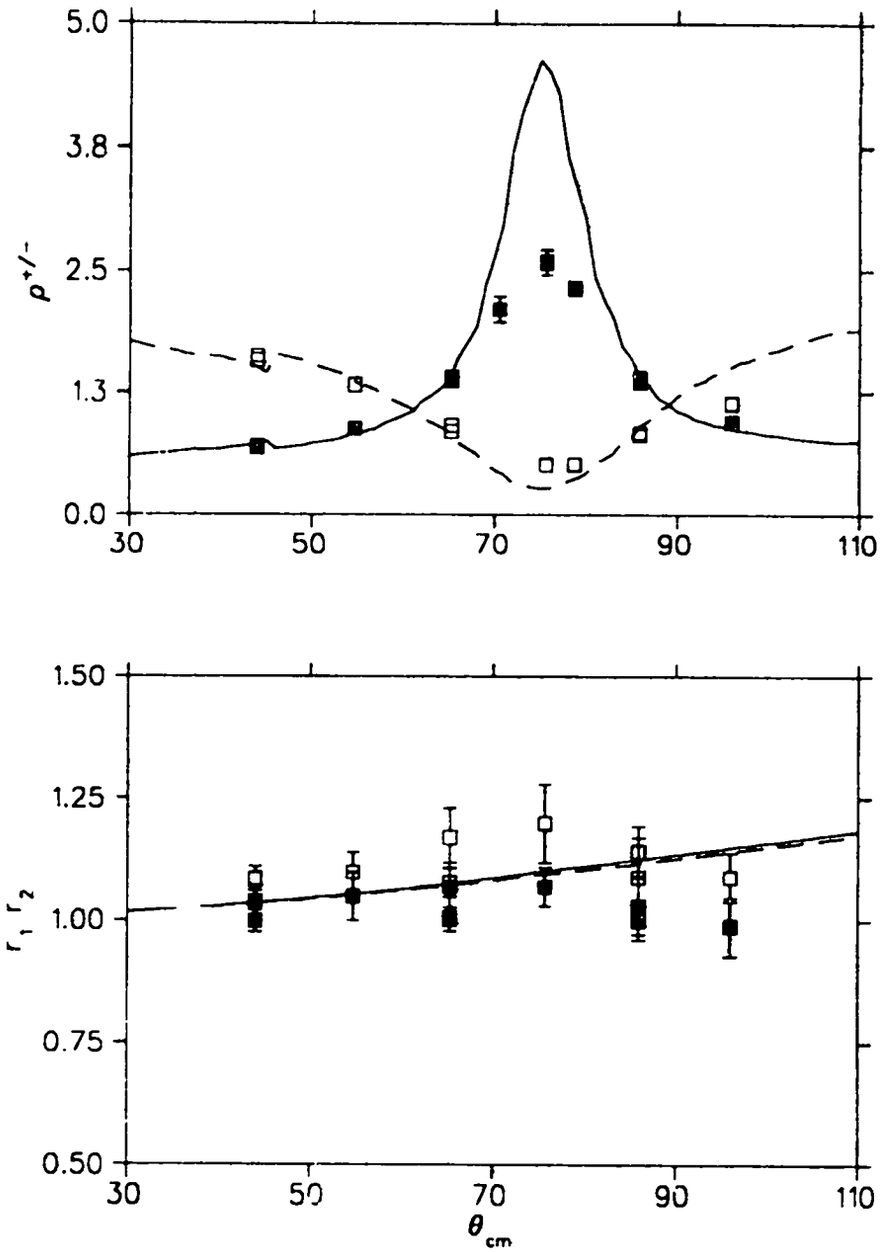

Figure 1.9: A fixed-scatterer impulse calculation of the 180 MeV ratios. *Top:* ρ^+ , filled squares, and ρ^- , open squares. *Bottom:* The charge symmetric ratios r_1 , filled squares, and r_2 , open squares. Data from previous experiments [Nef90],[Pil91],[Pil92] and [Ber91].

peaking spin-flip amplitude, and ρ^+ has a bump. The systematics are exactly the same for ρ^-, except that it is the numerator that goes as the non-spin-flip, and the denominator goes as the spin-flip amplitude, so ρ^- has a dip. The calculated values of ρ^+ and ρ^- match the data well. The size of the effect is somewhat too large at the depth of the dip, and the match is not good at large angles. This latter is expected since we are getting far out in momentum transfer, where the zero-momentum amplitudes (fixed-scatterer approximation) are less and less appropriate, because the kinematics require that scattering takes place from nucleons with higher momenta.

The match of the calculations with r_1 and r_2 is poor. At resonance energies, in the region of the NSF dip, r_1 is primarily

$$\frac{F_{pT}\ \ g(\pi^+ p)}{F_{n^3He}\ \ g(\pi^- n)};$$

the amplitudes should be nearly equal (in these calculations they are set equal, as the VPI program only calculates pion-proton scattering), and we may expect the form factor ratio to govern the shape here. The extrapolation to the neutron form factors is very crude· the subtlety of the effect is certainly beyond the calculation. The overall flatness of the curve is expected, but the steady rise is not seen in the data. At this energy and angle, r_2 is primarily

$$\frac{F_{pT}\ \ g(\pi^- p)}{F_{n^3He}\ \ g(\pi^+ n)};$$

neither numerator nor denominator are purely $I_z = \frac{3}{2}$. The hump in the data is not seen in the calculation. Both calculations are cut off at 110°, which is well beyond the possible momentum transfer from an at-rest nucleon.

Figure 1.10 shows a series of calculations of the ratios with different values or δ_e and δ_o. As the VPI phase-shift program only calculates amplitudes up to about 5 fm^{-2} (180° in the π-nucleon center of mass), the same amplitudes are used for π-nucleus center-of-mass angles from 110° through 180°. As ρ^+ and ρ^- depend so critically on the amplitudes, their values should not be taken seriously in the backward hemisphere. r_1 and r_2 are not so amplitude-dependent, and we might expect usable back-angle results for these latter two ratios. In the NSF dip region, the different values of δ_e and δ_o can cause small inflections if the proper combinations are chosen. However, this is not surprising as the NSF amplitudes are changing very rapidly here, and so a slight change in any parameter might be expected to have measurable effects. In the backward hemisphere, using different values of δ_e and δ_o change the magnitude, but not the shape, of r_1 and r_2.

In summary, the major features of the scattering at forward angles and resonance energies are well reproduced by the single-scatterer impulse approximation, as seen by the good match for ρ^+ and ρ^-. The calculation is good up to the region of the NSF dip, as expected. The calculation fails to reproduce the subtler features of r_1 and r_2, which are not so obviously related to the π-nucleon amplitude shapes.

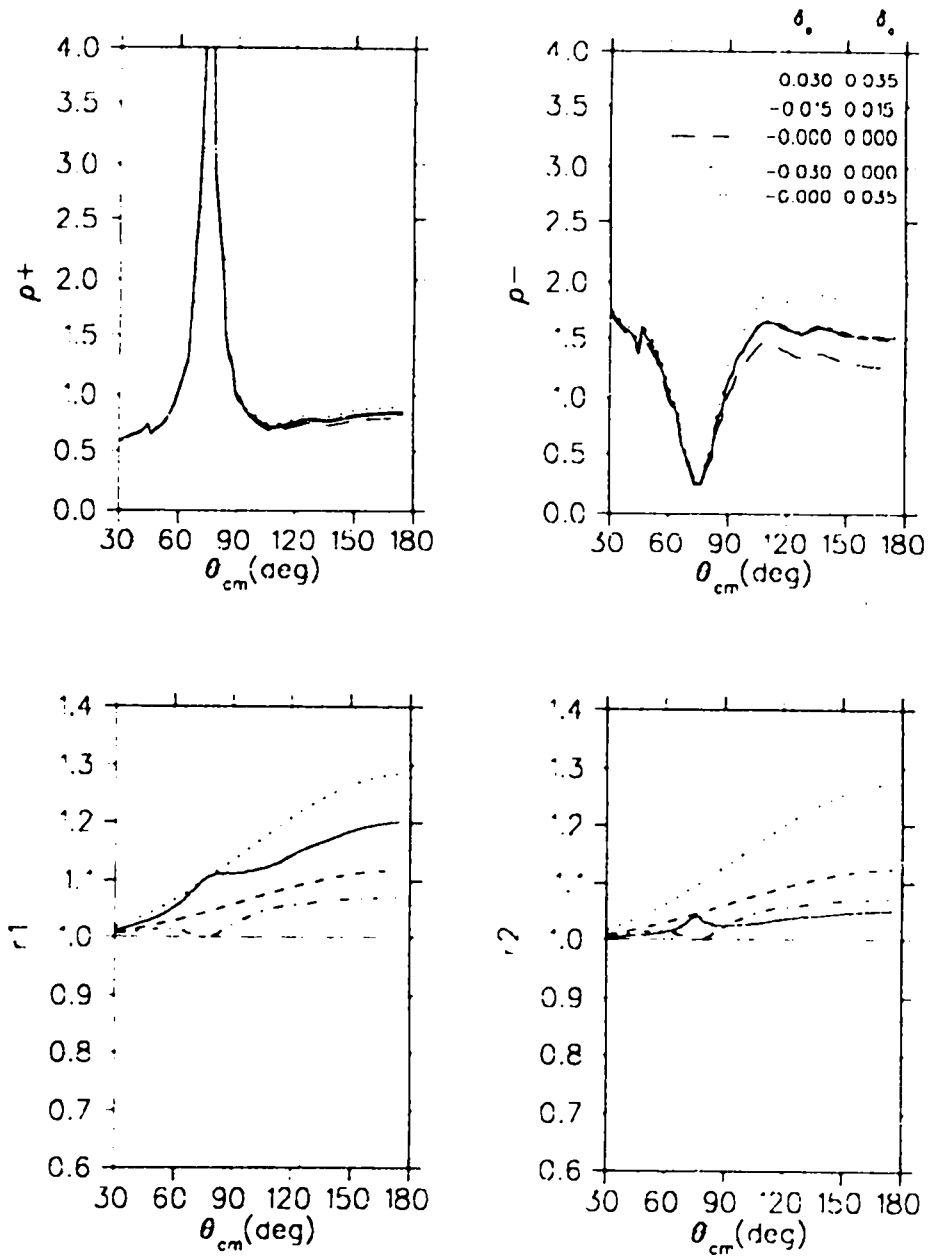

Figure 1.10: Simple model calculation of the ratios at 180 MeV for different values of δ_c and δ_o . Small changes can cause shape changes in the dip region and large variations in magnitude at back angles, for r_1 and r_2 . ρ^+ and ρ^- are not affected appreciably in the forward hemisphere.

1.6.5 The Optical Model

Using equations 1.12, we can derive a more general scattering result [Eis80, Chap.4]. We will be taking the expectation value of T between nuclear ground states and pion states,

$$< T >=< \sum_{i}^{A}(t_i + t_i G \sum_{j \neq i}^{A} T_j) > \sim < \sum_{i}^{A}(t_i + t_i G T) >,$$

assuming in the last line that making the sum over j include the i term would only give an error of order $1/A$. This is an acceptable result for large A; for A = 3, it is necessary to make a correction [Gib91] [Ker59]. Ignoring the pion states for now, we take the nuclear ground-state expectation value

$$\begin{aligned} < 0 \,|T|\, 0 > &= < 0 \,|\sum_{i}^{A} t_i|\, 0 > \\ &+ \sum_{\mu} < 0 \,|\sum_{i}^{A} t_i|\, \mu >< \mu \,|T|\, 0 >, \end{aligned}$$

where the summation over μ is over a complete set of nuclear states, and the subscript on G means that it has the nuclear energy H_μ in the denominator. We can separate the summation into two parts, $\mu = 0$ and $\mu \neq 0$. Then

$$\begin{aligned} < 0 \,|T|\, 0 > &= < 0 \,|\sum_{i}^{A} t_i|\, 0 > \\ &+ < 0 \,|\sum_{i}^{A} t_i|\, 0 > G_0 < 0 \,|T|\, 0 > \\ &+ \sum_{\mu \neq 0} < 0 \,|\sum_{i}^{A} t_i|\, \mu >< \mu \,|T|\, 0 >. \end{aligned}$$

We assume the final term is not as important as the other two because it involves transitions to excited states and then back to the ground state, and this is less likely than remaining in the ground state the whole time. Defining

$$V \equiv < 0 \,|\sum_{i}^{A} t_i|\, 0 >$$

we write

$$< 0 \,|T|\, 0 > = V + V G_0 < 0 \,|T|\, 0 >.$$

This is the form of the Lippman-Schwinger equation for the scattering matrix T for scattering from a potential V. Taking the Born approximation for the scattering amplitude

$$B = < \mathbf{k}' \,|V|\, \mathbf{k} >$$

is the first-order optical model. In pion scattering, it has been experimentally determined that a good approximation for the π-nucleon interaction is [Eis80, page 196]

$$< \mathbf{k}' \,|t(E_\pi)|\, \mathbf{k} > = b(E_\pi) + c(E_\pi)\mathbf{k}' \cdot \mathbf{k},$$

for spin and isospin saturated nuclei, with pion energies below 300 MeV. Assuming that the pion interaction is the same with each nucleon, we can rewrite Eq. 1.15 as [Eis80, page 195]

$$< \mathbf{k}' \,|V_c|\, \mathbf{k} > = A < \mathbf{k}' \,|t|\, \mathbf{k} > \int e^{i(\mathbf{k}-\mathbf{k}')\cdot\mathbf{r}} \rho(\mathbf{r}) d\mathbf{r}.$$

Kisslinger noted [Kis55] that this result would be obtained if

$$V_c = Ab(E_\pi)\rho(\mathbf{r}) - Ac(E_\pi)\nabla \cdot \rho(\mathbf{r})\nabla.$$

The problem is thus reduced to determination of b and c at a given energy, and for a given density.

Many groups have enlarged upon this idea, with potentials that include spin and isospin dependent parts, and sophisticated functions for the various coefficients introduced, including b and c above [Lan75], [Str79].

Some applications by other authors to the forward-hemisphere data from these experiments are discussed below.

1.7 Other Calculations

Several groups have calculated the cross sections, as well as some of the ratios. A few of these are considered below.

Nefkens *et. al.* performed an analysis of the forward-hemisphere data using an impulse approximation similar to the one performed in Sec. 1.6.4; that calculation was done after seeing Nefkens' work. The authors used the VPI phase-shift analysis for the π-nucleon amplitudes, and, in calculating the ratios, assumed an exponential shape for the form factors. They also include a shadowing factor designed to model the fact that the nucleon under consideration will be hidden by the other nucleons a certain fraction of the time. Assuming that $f(\pi^+ p) = 3f(\pi^- p)$ and $f(\pi^+ p) = f(\pi^- n)$, and assuming that the isomirror relations hold as well, and that these also hold for the spin-flip amplitudes, the authors derive the relationships

$$r_2 \sim (F_{nT} / F_{p^3He})^2 \text{ and}$$

$$F_{nT} = [1 + (0.03 \pm 0.02)q^2] F_{p^3He}.$$

The latter equation can be rewritten, assuming that the terms in the square brackets are the expansion of an exponential, as

$$F_{nT} = F_{p^3He}\, e^{0.03q^2} = F_{p^3He}\, e^{2\times 0.05\times 1.74 q^2/6},$$

that is $\delta_e = -0.05$, in rough agreement with the value found by Gibbs and Gibson (see Sec. 1.6.4 and below).

Electron scattering from ^{3}He has shown that there is a slight density depletion at $r = 0$ [McC77]. Equation 1.14 can be written as follows, if the density is assumed spherical:

$$F(q) \propto \int j_0(qr)\rho(r)r^2 dr$$

where j_0 is the spherical Bessel function. We can transform this and write

$$\rho(r) \propto \int j_0(qr)F(q)q^2 dq.$$

he integrand in the latter is a damped sine function; if we write the form factor as the sum of two gaussians, $F = F_1 + F_2$, we can match the density depletion well.

Barshay and Seghal[BarS5] have assumed a correlation among the nucleons in ^{3}He that allows them to fit a form factor written as the sum of two gaussians to the known form-factor shape. The diagram shown in Fig. 1.11 is from their paper. The np distance is the same in both nuclei in the figure, and by using this and defining the center of mass to be at the same place for both, they derive the equation

$$R_p^2 + 2R_n^2 = 3R_t^2.$$

Next, they define the form factors as

$$F^T = (1-\epsilon)e^{-R_1^2 q^2/6} + \epsilon e^{-R_t^2 q^2/6},$$

for the equal proton and neutron form factors of T, and

$$F_{p,n}^{He} = (1-\epsilon)e^{-R_2^2 q^2/6} + \epsilon e^{-R_{p,n}^2 q^2/6},$$

for the proton and neutron form factors of ^{3}He. R_1 and R_2 are the numbers that give the 'regular' gaussian form factors, that is they are the radii for uncorrelated nucleons. Using the correlation equation and the known values of the T and ^{3}He charge form factors from electron scattering, the authors determine the following values for the parameters:

$$\begin{aligned} \epsilon &= 0.27, \\ R_1 &= 1.67fm, \\ R_2 &= 1.74fm, \\ R_T &= 1.12fm, \\ R_p &= 1.31fm \text{ and} \\ R_n &= 1.02fm. \end{aligned}$$

The authors calculate r_1 and r_2 using the single-scattering impulse approximation given in Sec. 1.6.4, but they use only the p-wave part of the amplitudes, that

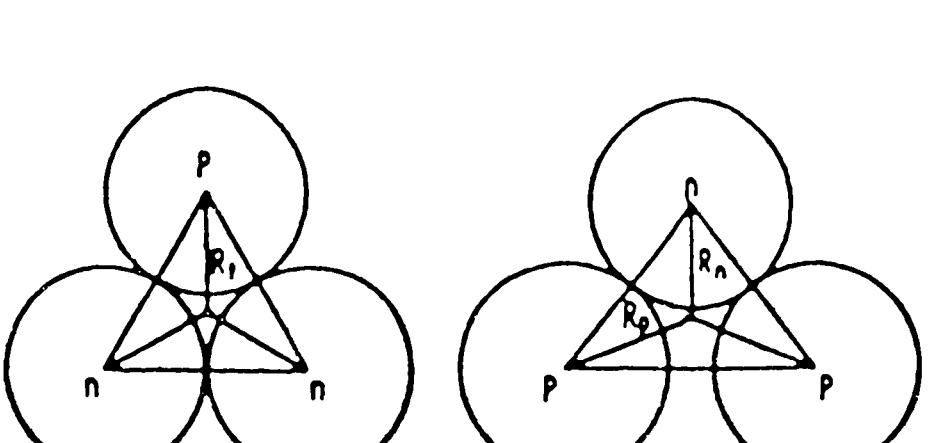

Figure 1.11: Figure from [Bar85], T on the left, and ^{3}He on the right. T is an equilateral triangle, with nucleon radius R_t. ^{3}He is an isosceles triangle with proton and neutron radii R_p and R_n, respectively.

is

$$
\begin{aligned}
f(\pi^+ p) &= f(\pi^- n) = 2\cos(\theta), \\
f(\pi^+ n) &= f(\pi^- p) = \frac{2}{3}\cos(\theta), \\
g(\pi^+ p) &= g(\pi^- n) = \sin(\theta) \; and \\
g(\pi^+ n) &= g(\pi^- p) = \frac{1}{3}\sin\theta.
\end{aligned}
$$

Figures 1.12 and Fig. 1.13 reproduce the authors' calculations (on the left in each figure), and show the same calculations done using the VPI-phase-shift amplitudes instead of the p-wave forms, (on the right in each figure). Note that the authors did not calculate ρ^+ or ρ^- , but as they gave the values for all of their parameters, it is easy to do the calculation using their method; this is done here. Their r_2 result is especially intriguing as the bump and return to 1.0 is reproduced fairly well. Their r_1 calculation has a similar but smaller bump; the shape is similar to that reported by Exp. 546 (□, [Nef90]), but the other data, taken with the new targets and using Deuterium for normalization cross sections (×, [Pil91] and ◇, [Pil92], [Ber91]), are flatter, and further from the calculation. Their ρ^+ and ρ^- results are shifted from the data, but have the correct shapes otherwise. The calculation was redone, using the VPI amplitudes with the authors' form factors; the results are shown on the right in each figure. ρ^+ and ρ^- are now a good match for the data, but r_2 no longer comes back to 1.0 after the hump. There is still a slight inflection; evidently the good match in the authors' result was somewhat fortuitous, as smoothing out the cosine dependence by including other than p-waves eliminates the good match with the data.

Kim, Krell and Tiator [Kim86] and Kim, Kim and Landau [Kim87] have done optical model calculations in an attempt to explain the forward-angle ratios. In their calculations, they consider only the Coulomb interaction as a source of CSB.

The first of these papers looks at both nuclear-Coulomb interference and Coulomb repulsion of the protons of ^{3}He; no spin dependence is included in the calculation. The densities are exponentials

$$\rho_p(r) = N_p e^{-\frac{3}{2}r^2/r_p^2}, \; \rho_n(r) = N_n e^{-\frac{3}{2}r^2/r_n^2},$$

where the subscripts n and p refer to neutrons and protons respectively, and N is the number of nucleons of a type, either neutrons or protons. The authors find a nuclear-Coulomb interference-related structure in r_1 , r_2 , and R, around 90° in the π-nucleus center of mass, which is well beyond the $\sim$ 78° location of the NSF dip, with CSB due only to Coulomb interference, and not proton repulsion. When they include proton repulsion in ^{3}He, by increasing r_p by 0.03 fm in ^{3}He, they see a similar structure; this addition makes r_1 , r_2 and R greater than 1.0 in the backward hemisphere. In both cases, the backward hemisphere ratios are smooth and structureless. These calculations, which are sketched over the data

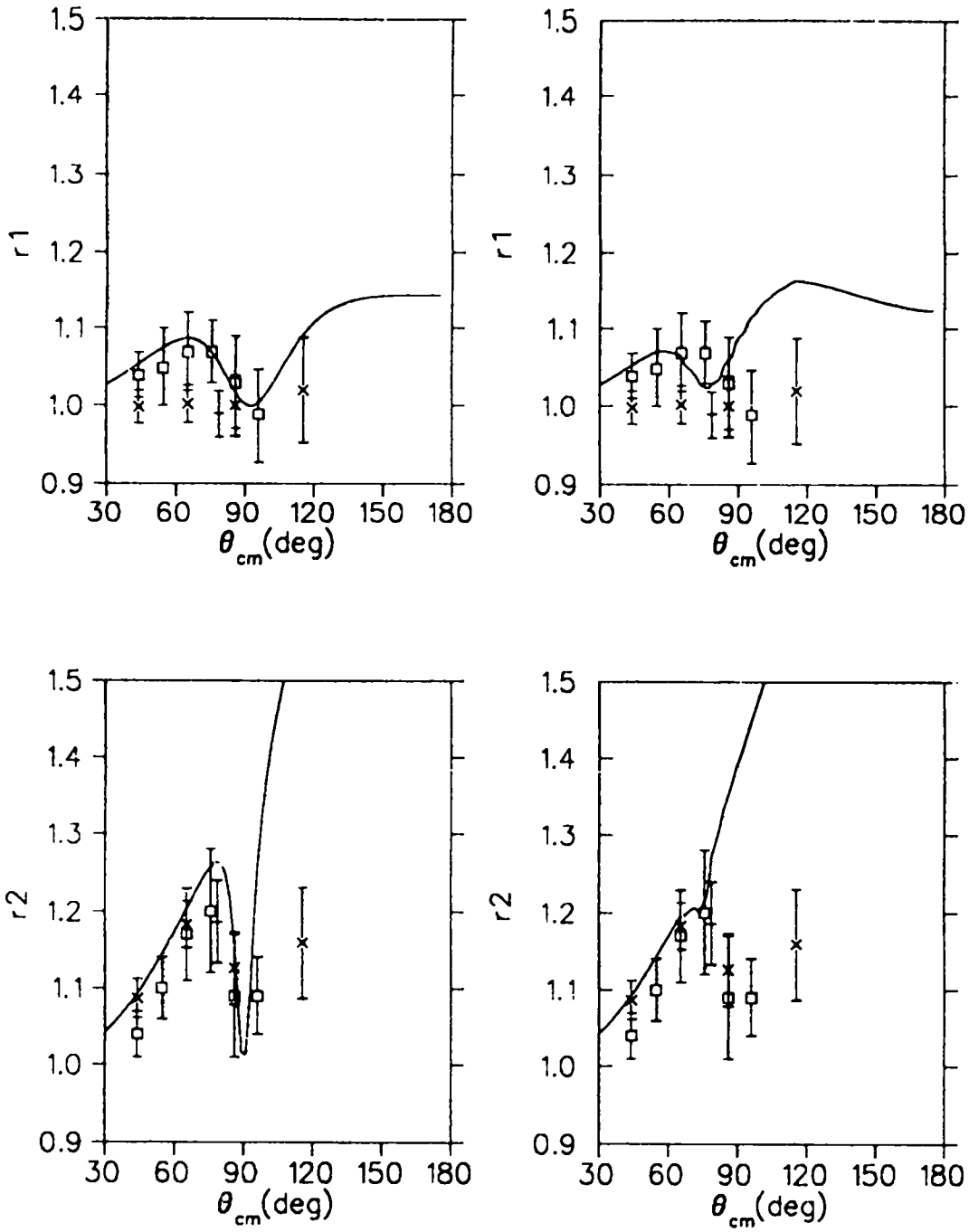

Figure 1.12: r_1 and r_2 calculated in a single-scattering impulse approximation, using sum-of-gaussian form factors, from [Bar85]. *left:* Using p-waves only. *right:* Using VPI-phase-shift amplitudes. The bump in r_2 is reproduced fairly well using the p-wave-only formulation.

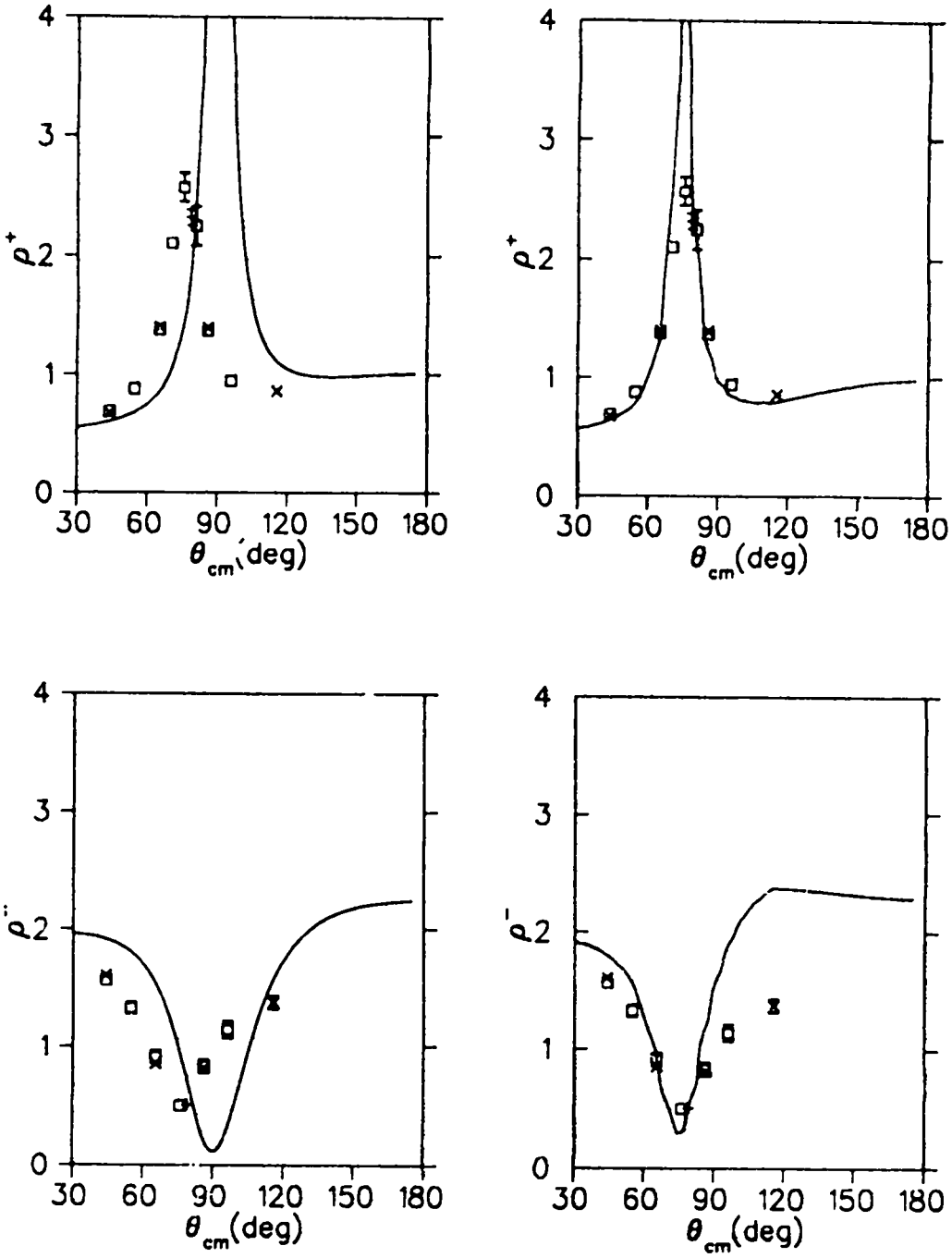

Figure 1.13: ρ^+ and ρ^- , using sum-of-gaussian for factors from [Bar85] and a single-scattering impulse approximation. *left:* p-wave-only amplitudes. *right:* VPI-phase-shift amplitudes.

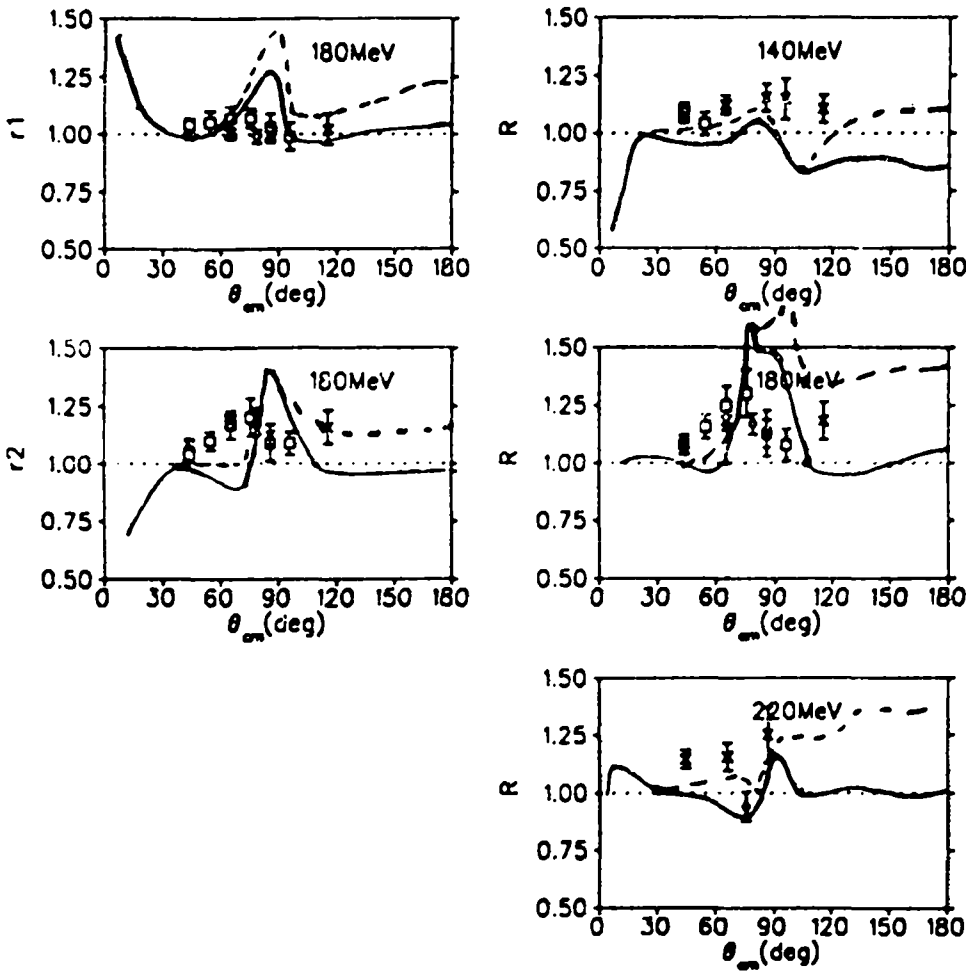

Figure 1.14: Ratio calculations by Kim, Krell and Tiator [Kim86], sketched over the data. The solid lines are their calculation for π-nucleus scattering including Coulomb interference, but no Coulomb repulsion in ^{3}He. For the dotted lines, they add Coulomb repulsion in the form of an additional 0.03 fm separation in the ^{3}He-proton radius. The data available when this calculation was done was only from experiment 546. □ Exp. 546 [Nef90], × Exp. 905 [Pil91], ◇ Exp. 1032 [Pil92] and [Ber91].

in Fig. 1.14 which was taken from the reference, show that while the calculation does not represent the data very well, the nuclear-Coulomb interference should not be ignored, and that at least at back angles, the optical-model calculation is very sensitive to the nucleon separation, which means that it is very sensitive to the form factors.

The second paper [Kim87] considers only nuclear-Coulomb interference as a source of CSB. The authors use a momentum-space optical potential, which includes spin-flip interactions. They do a credible job on R on the large-angle side, matching the slope and coming back to 1.0 around 100° in the π-nucleus center of mass, where they found the nuclear-Coulomb interference structure in the previous paper. The rest of the angular region is not a very good match. Specifically, their curves are very flat between 30° and 65°, where the data show a significant deviation from 1.0 with a smooth slope in r_2 , and consequently in R. Their bump is too narrow in r_2 and R; however the height is in keeping with the later data sets ($\diamond$, $\times$) and they find the peak at the right location (around 78° in the π-nucleus center of mass). In their previous paper, added proton separation in ^{3}He gave some deviation from 1.0 in the region forward of the NSF dip, and some added deviation and shape in the backward hemisphere; possibly this lack explains the corresponding lack in these regions in the second paper. Figure 1.15 is a sketch of their results over the existing data. Kim *et. al.* claim to have shown that the structure in R in the NSF dip region is due solely to Coulomb interference. However, as suggested by Briscoe and Silverman [Bri89], considering that they have only identified a structure whose location is near the NSF dip, while missing the amplitude and width of the structure as well as failing to reproduce the rest of the data, it seems more reasonable to say that they have shown that Coulomb interference has a non-negligible effect in this region, and should be included in any complete treatment.

A more recent momentum-space optical-model calculation has been performed by Gibbs and Gibson [Gib91]. Their calculation includes spin-flip scattering and Coulomb scattering and repulsion. They calculate cross sections and R. They state that the major dependence found in their scattering calculation was on the neutron and proton radii. Actually, they assume that the proton radii are known from elastic electron scattering, and they search for values of δ_e , which is the difference between the neutron radius in T and the proton radius in ^{3}He, and δ_o , which is the difference between the neutron radius in ^{3}He and the proton radius in T. For each combination of the scattering-theory parameters, they perform a chi-square fit to the data to determine the best values of δ_e and δ_o . Their results are

$$\delta_e = -0.030 \pm 0.08 fm$$

and

$$\delta_o = 0.035 \pm 0.07 fm.$$

Figure 1.16 shows their calculation of R : they do a reasonable job on the forward

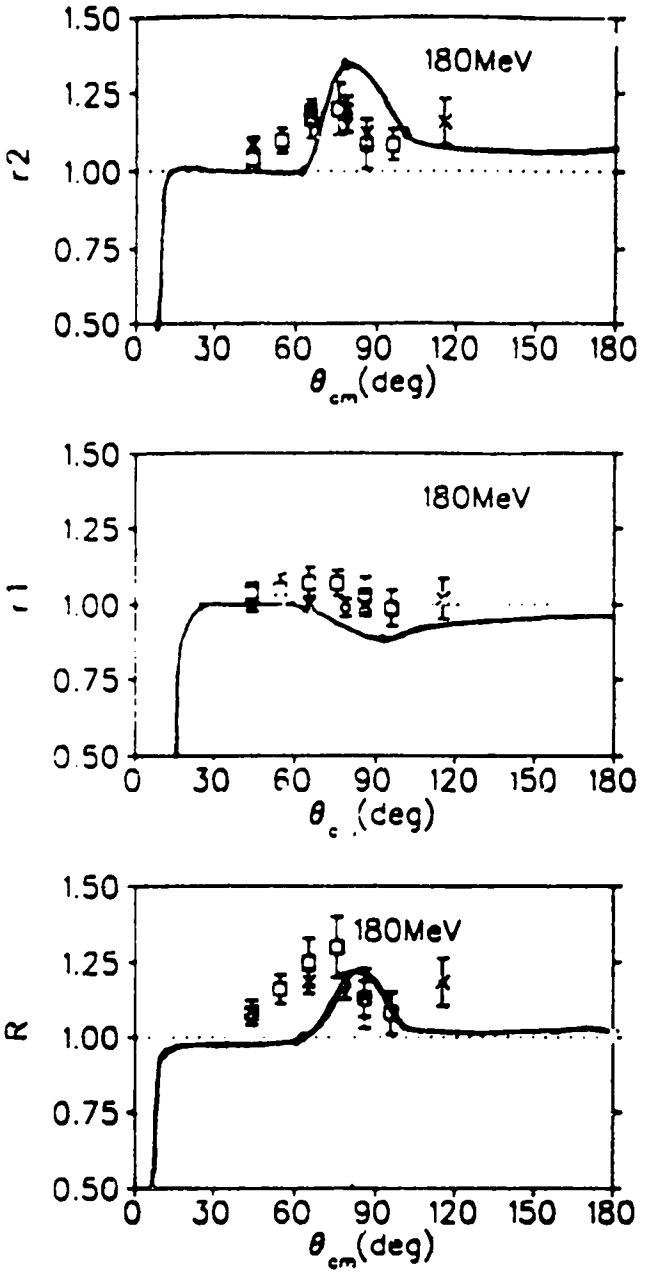

Figure 1.15: Calculations by Kim, Kim and Landau [Kim87]. CSB is included by nuclear-Coulomb interference only. The large-angle slope of R is well represented, in the region that the authors previously found the interference related structure in R. Only the experiment 546 data was available at the time of the calculation. □ Exp. 546 [Nef90], × Exp. 9C [Pil91], ◇ Exp. 1032 [Pil92] and [Ber91].

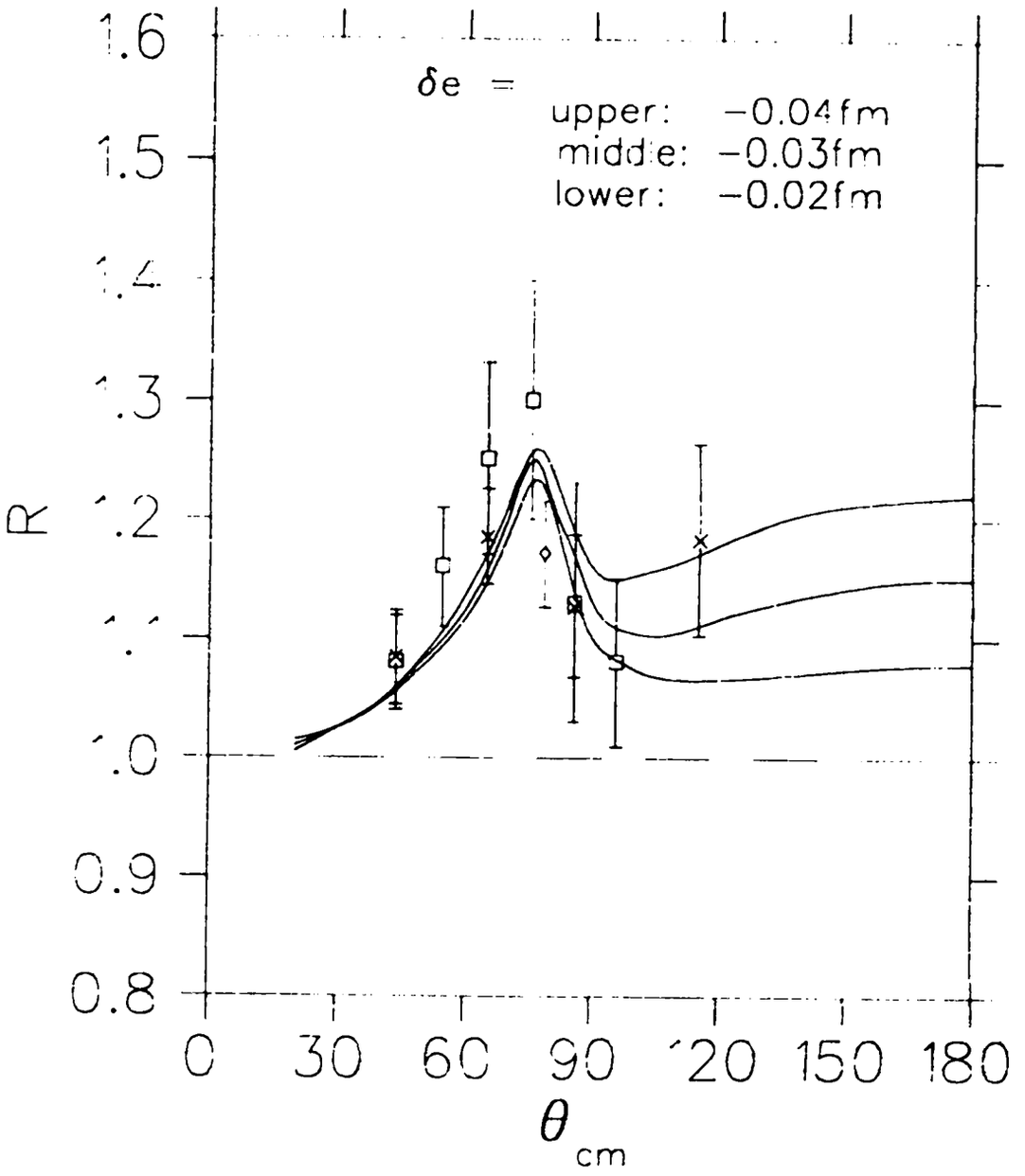

Figure 1.16: R from Gibbs and Gibson[Gib91]. The three curves show the effects of varying δ_e by $\pm .01$ fm, assuming $\delta_n = 0.035$ fm. □ Exp. 546 [Nef90], × Exp. 905 [Pil91], ◇ Exp. 1032 [Pil92] and [Ber91].

hemisphere data. Variations of 0.01 fm in δ_2 make a noticeable change in their backward hemisphere curves.

Figure 1.17 shows their cross section calculations, using the parameters that gave the best R results. They have produced a good match in the dip region, although a little high for π^{+3}He. The similarity of the symmetric pairs is obvious (diagonal from each other in the figure).

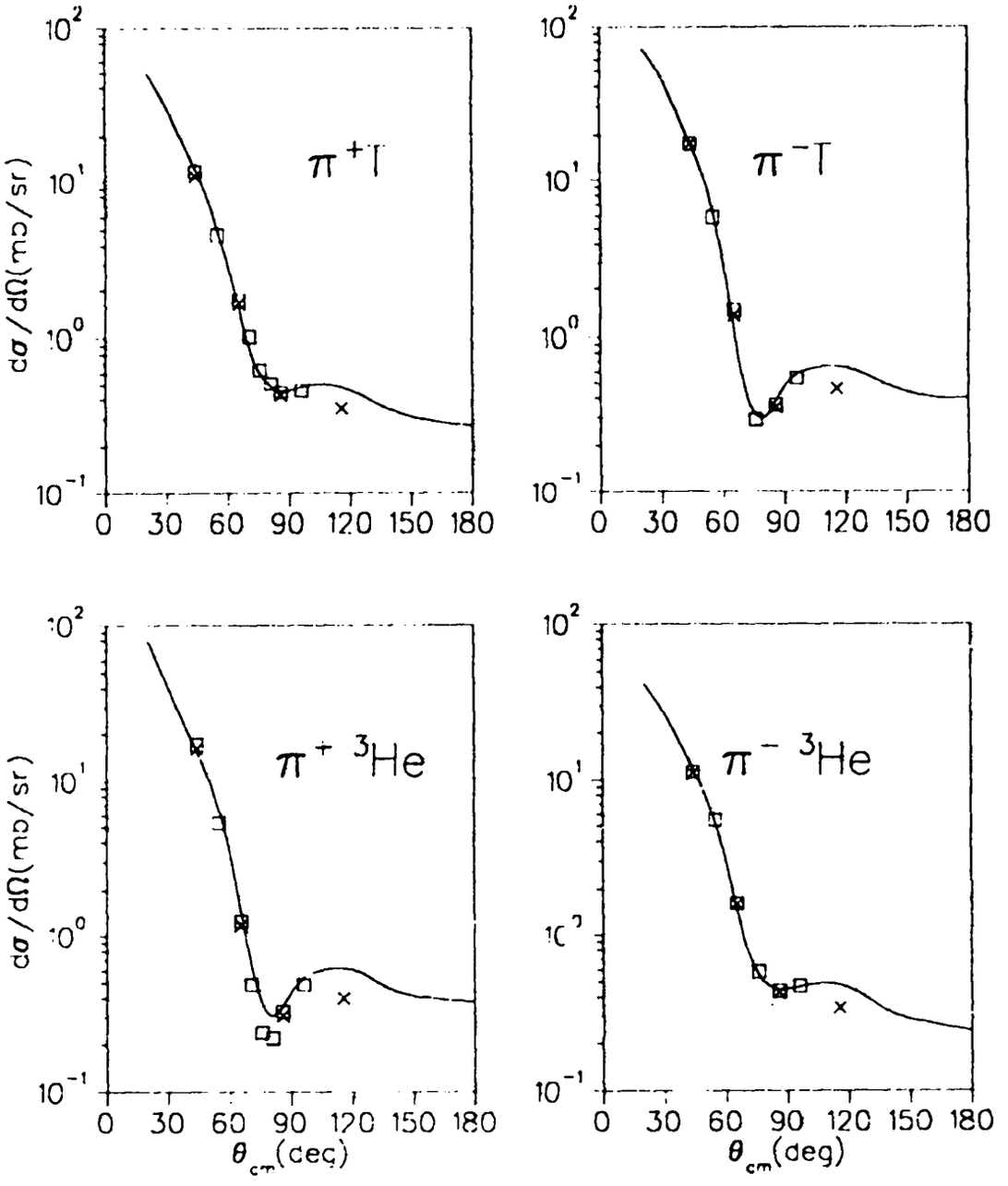

Figure 1.17: Cross section calculations from[Gib91]. The dip region is reproduced quite well. □ Exp. 546 [Nef90], × Exp. 905 [Pil91], ◇ Exp. 1032 [Pil92] and [Ber91].

1.8 Summary

The most dramatic features of the forward-hemisphere results are due to the NSF dip. The simple ratios ρ^+ and ρ^- were well-reproduced by the Simple-Model calculation done in Sec. 1.6.4; the most important input was the π-nucleon amplitudes, which were taken from the VPI phase-shift analysis, assuming a non-moving nucleon. The calculation failed to reproduce the bump in r_2 . In that calculation, Backward-hemisphere values of r_1 and r_2 depend mostly on the radii used in the exponential form factors. Kinematical considerations indicate that multiple scattering should be relatively more important in the backward hemisphere.

Calculations by Kim and collaborators [Kim86] [Kim87] failed to reproduce the ratios but did show that Coulomb interference could make important contributions in the region of the NSF dip.

Finally, calculations by Gibbs and Gibson [Gib91] yielded precise values of δ_e and δ_o and matched the forward-hemisphere cross sections and R data quite well. This calculation included Coulomb interference in a potential interaction model. The authors state that they need to include NCSB in the form of added proton repulsion in a nuclear model in order to reproduce the values of ρ^+ and ρ^- found in the scattering calculation.

Backward-hemisphere measurements will extend the pion-elastic scattering data from T and ^{3}He into previously uncharted regions. Data taken farther from the NSF dip will not suffer the difficulties due to the steeply changing amplitudes in this region, and so it may be possible to understand systematics of the scattering calculations that are obscured near the dip. As the scattering angle approaches 180°, the spin-flip amplitudes approach zero, and comparisons with scattering from spin-zero nuclei, specifically ^{4}He, might be revealing.

The question of charge-symmetry breaking remains. In the backward hemisphere, we might expect to benefit from a lack of Coulomb interference, if this latter is primarily manifested in the region of the NSF dip, as suggested by the authors mentioned in Sec. 1.7. However, the expected increase in the importance of multiple scattering in the backward hemisphere may introduce complications that outweigh the benefits.

Historically, measurement of the excitation function near 180° (Experiment #1064) was proposed to and accepted by the LAMPF Program Advisory Committee before the angular distribution experiment (Experiment #1155) was proposed. The proposal for Exp. 1064 [Bri86] stated that the primary purpose of the experiment was to provide πT and π^3He cross-section data in kinematical regions previously uncharted for these nuclei. It was noted that comparison of the charge-symmetric ratios near the NSF dip, where non-spin-flip scattering is nearly zero, to the ratios measured near 180°, where nearly all of the single scattering is spin-flip (recall the sine dependence of the spin-flip amplitudes), might show the relative amounts of NCSB in the spin-flip and non-spin-flip amplitudes.

The primary justification for Exp. 1155 [Bri87] was a series of preliminary

calculations by Gibbs and Gibson [Bri87] showing that a R calculation at 180 MeV would be rather insensitive to model variations in the description of the π-nucleon force, and would depend mostly on the nuclear radii chosen for the nucleons in T and ^{3}He. They stated that a complete angular distribution, and thus a complete measurement of the momentum-transfer dependence of the problem, would be necessary to correctly derive the radii (recall that the radius and momentum transfer are related through the form factors). These preliminary calculations eventually led to the full calculation and back-angle predictions discussed in Sec. 1.7.

The goal of this work is to provide the back-angle excitation-function and angular-distribution data needed, to extend the data base, to test the backward-hemisphere predictions of the authors discussed in Sec. 1.7, and to explore the relative CSB of the non-spin-flip amplitudes.

Chapter 2

Experimental Equipment and Setup

2.1 Introduction

The experiments were performed over a six week period in the summer of 1989, using the Energetic Pion Channel and Spectrometer (EPICS) at the Clinton P. Anderson Meson Physics Facility (LAMPF), which is a part of the Los Alamos National Laboratory, in Los Alamos, New Mexico. In addition to the standard EPICS setup we used an extra bending magnet, a special target changer and high-pressure gas targets.

2.2 LAMPF

LAMPF is a quarter-mile-long proton accelerator that produces a beam of 800-MeV protons at currents of up to 1000 μa. In addition to the main proton beam (H^+), H^- ion beams can be transported on the opposite phase of the RF. The H^- beams serve the proton and neutron scattering areas, and can be polarized for some applications; these latter beams were not used in these experiments.

The protons are focused on graphite production targets to produce secondary pion beams. Pions of various momenta are selected by magnetic optical systems ('channels') which have entrances at angles to the proton beam downstream of the targets; the angles are selected to maximize pion flux in a given momentum range. Different pion channels produce pion beams with different qualities, such as special energy ranges and linearly dispersed momentum. The pion beams are focused on nuclear targets, and the scattering-reaction products are analyzed in order to understand the reaction processes and ultimately the nuclear structure of the targets.

2.3 EPICS

2.3.1 Channel and Spectrometer

The EPICS channel produces a pion beam with an energy range of 70 - 300 MeV. The beam is 8 cm wide and 20 cm high with a vertical momentum dispersion of $10 cm/percent$. The rate for π^+ is about 3×10^7 *per* second at 70 MeV and increases to about 26×10^7 *per* second at 290 MeV. Rates for π^- are about one-fifth of the π^+ rates, depending on the beam energy; the ratio reflects the relative production rate in the graphite target. The beam is monitored in several ways. There is a toroid upstream of the production target in the proton line which monitors the proton current. Since the pion production at any particular energy and angle (the angle of the channel relative to the proton beam) is proportional to the proton current, the toroid current is proportional to the pion current. However, if the primary proton beam is shifted slightly due to tuning changes in the accelerator, it will hit the production target at a slightly different angle and location, causing the pion flux and angle to change as well. Therefore the proportionality constant between the pion beam current and that of the proton beam, as measured by the toroid, is dependent on the proton-beam steering at the production target.

The second monitor is an ion chamber in the production-target box that views the graphite production target. As the ion-chamber current is proportional to the proton-beam current, using the former to normalize the pion beam has the same problems as using the toroid does. This monitor failed during the experiment; it has not been used for any quoted results.

The primary pion-beam monitor is an ion chamber that views the pion beam directly. It is mounted on a stand in the experiment area and intercepts the beam after it passes through the target and scattering chamber. This ion chamber is faced with a 1-inch graphite slab to reduce the number of protons that are detected (protons are present in the π^+ beam from scattering of the proton beam on the production target). The current from the ion chamber is proportional to the total energy deposited by all the charged components of the beam: muons, electrons, protons and pions. Since these constituents are in constant proportion to each other at each energy, the ion-chamber current is proportional to the pion current at each energy.

Seestrom [See81] found that there is a proportionality inconsistency between π^+ and π^-. Quantifying this difference requires a detailed knowledge of the pion-beam composition and its interaction with the ion-chamber gas. This is not important in these experiments, because all cross sections and cross-section ratios have yields of like polarity in both their numerators and denominators, so the proportionality constants cancel (see Chap. 3).

Protons can be removed from the pion beam by moving one or more polyethelene or beryllium degraders into the beam in the channel. A proton traversing the degrader loses more energy than a pion of the same momentum. After the

traversal, passing the beam through a bending magnet separates the lower momentum protons from the pions. The protons miss the target at the end of the channel and are lost. In this experiment, the protons and the pions were not kinematically matched after scattering, that is the scattered protons had too little momentum to make it through the spectrometer, so the degraders were not used.

The channel terminates at the scattering chamber, which holds the target in vacuum. The channel and scattering chamber are often vacuum coupled, but the scattering chamber used in the back-angle setup for these experiments rotates with the spectrometer pivot, and no provisions have been made to provide coupling. Instead, the beam pipe was terminated with a thin Kapton window. A few-inch air gap separated it from the mylar window of the scattering chamber, which was 25 cm × 120 cm by 0.038 cm thick. The mylar was epoxied to an aluminum frame, and this frame was bolted to the window frame of the scattering chamber. Entries to the scattering chamber required releasing the vacuum and removing the frame, which flexed the window and glue. A new window was required every few entries.

The spectrometer is mounted on air pads and can be rotated up to a floor angle of 120° relative to the beam. It consists of two large dipoles that bend the beam in a vertical plane for momentum analysis and a quadrupole triplet at the spectrometer's entrance to provide point to point focusing in the vertical plane, which maintains the momentum dispersion of the incoming beam, and point to parallel focusing in the horizontal (scattering) plane. The coordinate system at EPICS is right handed with the positive z-direction along the beam. The x axis is positive downward and the y axis is positive to the left, looking downstream.

Particle tracks are monitored with three groups of wire chambers. The first group brackets the focal plane of the quadrupole triplet, one x-direction and one y-direction chamber upstream and the same x-y combination downstream, allowing determination of the x and y position of a particle track as well as the angle of the track with respect to the central ray. After the dipoles four x-y pairs are used to analyze the position and angle again.

Three scintillators provide event timing. The first (S_1) is just before the front chambers, and the second and third (S_2, S_3) are behind the last chambers. A good event must be seen by at least one pair of front chambers and the two rear scintillators; this combination forms the trigger. S_1 can be removed from the flight path, as was done for this experiment. When S_1 is left in, it is included in the trigger as well. A time-of-flight correction is done between the front and rear detectors based on the particle's energy as well as its calculated flight path length, in order to reference events in the front and rear of the spectrometer to a common time.

Figure 2.1 is a schematic diagram of the EPICS spectrometer, seen in the vertical plane. A hardware trigger is made from signals from several component detectors of the spectrometer. If each of these detectors outputs a logical signal simultaneously, it indicates that a particle has passed through the complete spec-

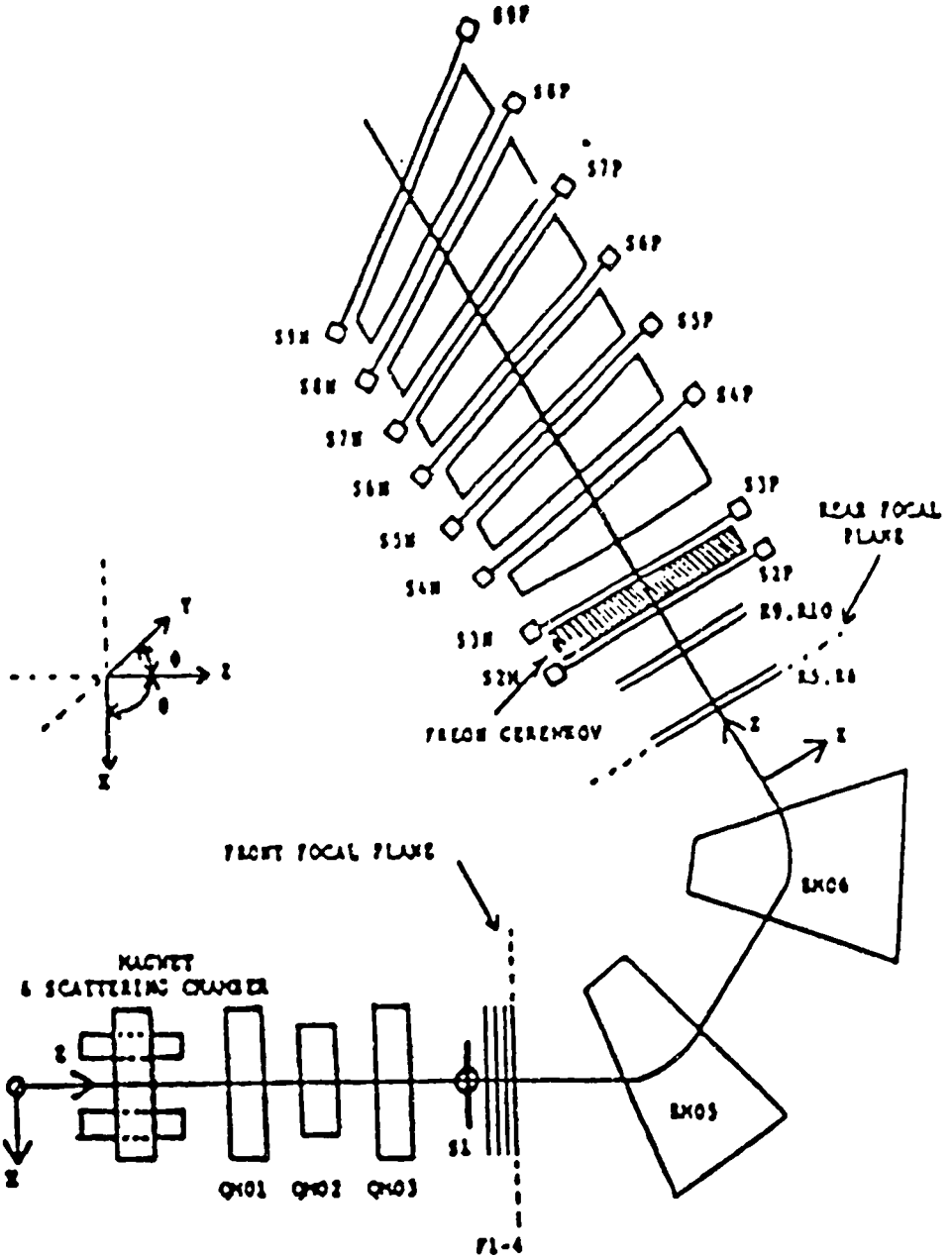

Figure 2.1: A schematic view of EPICS from the side.

trometer. A logical AND is formed and input to the LAMPF trigger module, which is a rack mounted module with several inputs. In response to an input, such as the event trigger, the trigger module signals the data-acquisition systems, over the data bus, that it has an event to be processed, and indicates the event's priority. Recently, a buffering capability has been added that allows up to 15 events to be stored and read out later. The LAMPF beam structure has a pulse that lasts for about 10% of the RF cycle, so that data can be stored during the pulse, and then read out from the buffers during the time between pulses.

The detector outputs are processed by time-to-digital (TDCs) converters, which digitize the time between start and stop pulses, and analog-to-digital converters (ADCs) which measure pulse height. Also, scalar registers keep count of pulses from discriminated detectors and current digitizers. This data is stored in the buffers and read out for each event. Readout is controlled by a LAMPF Micro-programmable Branch Driver (MBD), and the events are processed and written to tape by a micro-Vax computer.

On-line analysis is also possible for most of the events, depending on the data-taking rate. The angle, momentum, and target location of each scattering event are calculated using the wire chamber information (see Sec. 2.3.3). The excitation energy of the target nucleus, 'missing mass', is calculated from these results, and all of the calculated and raw data are histogrammed and can be displayed immediately.

2.3.2 Wire Chambers

EPICS has six x-chambers and six y-chambers. Their construction, calibration, and operation are discussed in [Ate81] and [Mor82]. They are drift chambers with interleaved sense and field wires. The signal wires are 0.8 cm apart, so that each drift cell is 0.4 cm. Each anode wire is connected to a delay line. Both ends of the delay line are read out, and each is used as a TDC stop; the times recorded for the two ends are called t_1 and t_2. A sum ($t_1 + t_2 \equiv t_s$) and a difference ($t_1 - t_2 \equiv t_d$) are formed for each event. The sum is the time it takes the signal to propagate from one end of the delay line to the other plus the time between the start and the actual event, plus twice the time it took the signal to get through the drift cell and down the signal wire to the drift line. If we assume that propagation down the signal wire is instantaneous, then t_s equals the drift time plus a constant. For EPICS chambers, we assume that each drift cell is uniformly illuminated, which is reasonable for such small cells. Then, the number of particles seen per unit drift time is

$$\frac{dN}{dt} = \frac{dN}{ds}\frac{ds}{dt} = cv(t)$$

where s is the drift cell position. Integrating gives

$$s(t) = \frac{1}{c}\int_0^t \frac{dN}{dt}dt$$